AD-A031 747 AIR FORCE INST OF TECH WRIGHT-PATTERSON AFB OHIO F/G 20/12
A CALCULATION OF THE HIGH TEMPERATURE TRANSPORT PROPERTIES OF Z--ETC(U)
MAY 76 T C GENONI

UNCLASSIFIED AFIT-CI-7T-1 NL

1 OF 1
AD A031747

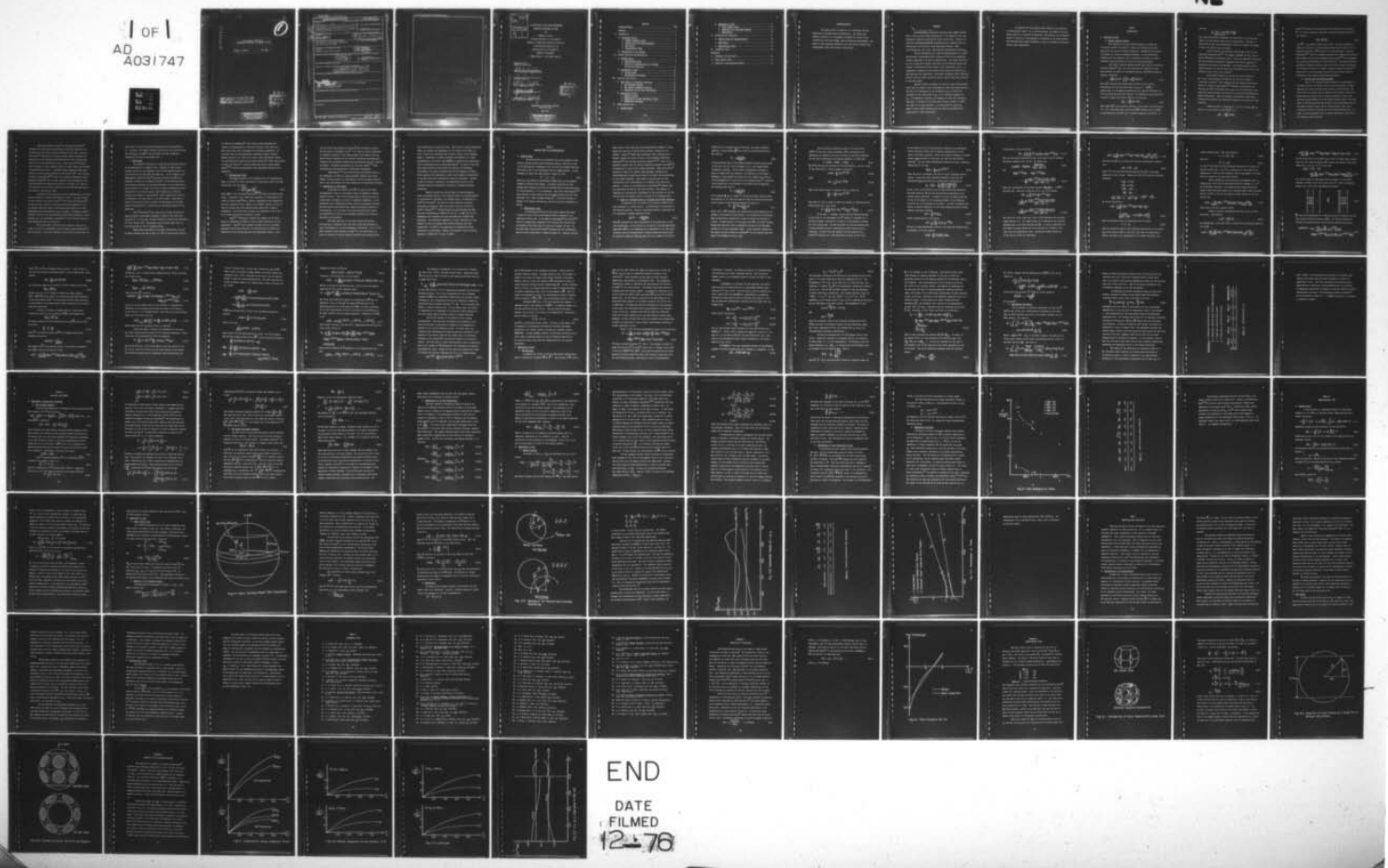

END

DATE FILMED
12-76

CI-7T-1

A CALCULATION OF THE HIGH TEMPERATURE TRANSPORT PROPERTIES OF ZINC

THOMAS C. GENONI

MAY 1976

UNCLASSIFIED

SECURITY CLASSIFICATION OF THIS PAGE (When Data Entered)

REPORT DOCUMENTATION PAGE		READ INSTRUCTIONS BEFORE COMPLETING FORM
1. REPORT NUMBER CI 7T-1	2. GOVT ACCESSION NO.	3. RECIPIENT'S CATALOG NUMBER
4. TITLE (and Subtitle) (6) A Calculation of the High Temperature Transport Properties of Zinc.		5. TYPE OF REPORT & PERIOD COVERED PhD Thesis 6. PERFORMING ORG. REPORT NUMBER
7. AUTHOR(s) (10) THOMAS C. GENONI CAPTAIN, USAF		8. CONTRACT OR GRANT NUMBER(s) (9) Doctoral thesis,
9. PERFORMING ORGANIZATION NAME AND ADDRESS AFIT Student at Rensselaer Polytechnic Institute, Troy, New York		10. PROGRAM ELEMENT, PROJECT, TASK AREA & WORK UNIT NUMBERS
11. CONTROLLING OFFICE NAME AND ADDRESS AFIT/CI Wright-Patterson AFB OH 45433		(11) 12. REPORT DATE May 1976 13. NUMBER OF PAGES 79 pages
14. MONITORING AGENCY NAME & ADDRESS (if different from Controlling Office) (12) 87p.		15. SECURITY CLASS. (of this report) Unclassified 15a. DECLASSIFICATION/DOWNGRADING SCHEDULE

16. DISTRIBUTION STATEMENT (of this Report)

Approved for Public Release; Distribution Unlimited

(14) AFIT-CI-7T-1

17. DISTRIBUTION STATEMENT (of the abstract entered in Block 20, if different from Report)

18. SUPPLEMENTARY NOTES

APPROVED FOR PUBLIC RELEASE AFR 190-17.

JERRAL F. GUESS, Captain, USAF
Director of Information, AFIT

19. KEY WORDS (Continue on reverse side if necessary and identify by block number)

20. ABSTRACT (Continue on reverse side if necessary and identify by block number)

Attached

DD FORM 1 JAN 73 1473 EDITION OF 1 NOV 65 IS OBSOLETE

012 200 LB

SECURITY CLASSIFICATION OF THIS PAGE (When Data Entered)

A CALCULATION OF THE HIGH TEMPERATURE TRANSPORT PROPERTIES OF ZINC

by

Thomas C. Genoni

A Thesis Submitted to the Graduate
Faculty of Rensselaer Polytechnic Institute
in Partial Fulfillment of the
Requirements for the Degree of
DOCTOR OF PHILOSOPHY
Major Subject: Solid State Physics

Approved by the
Examining Committee:

H B Huntington
H. B. Huntington, Thesis Adviser

E Brown
E. Brown, Member

P. A. Casabella, Member

E. J. Winhold, Member

Joseph E. Flaherty
J. E. Flaherty, Member

Rensselaer Polytechnic Institute
Troy, New York

May 1976

CONTENTS

ACKNOWLEDGEMENTS

The author wishes to thank Dr. H. B. Huntington for the opportunity of working under his supervision. The insight and guidance provided by Dr. Huntington throughout the course of this research have been most helpful, and are gratefully acknowledged. The author is also especially grateful to his wife for her patience and encouragement during the writing of this thesis.

ABSTRACT

This document applies ~~We have applied~~ a Nearly Free Electron Model (NFEM) combined with a local pseudopotential approximation to the analysis of the high temperature transport properties of single crystal Zinc. Within this framework, ~~we have been able to~~ it obtains qualitative agreement with the experimental observations of three anisotropic effects: self-electromigration, Hall effect, and diffusion thermoelectric power.

The electromigration of a weak scattering impurity in a Bloch electron gas is reconsidered while taking into account the conduction electron screening in the Hartree approximation. Our formal expression for the driving force depends explicitly on the dielectric matrix, and reduces to previously derived formulas in the appropriate limits. An approximate evaluation of the formulas yields values for Z_a^* and Z_c^* in good agreement with experiment. Anisotropic relaxation times, resulting from the observed phonon dispersion curves, tend to favor mass transport in the basal plane.

The Hall effect is analyzed in terms of a model Fermi surface based upon the standard 2-OPW (Orthogonalized Plane Wave) approximation. The effect of $\vec{k}$ dependence of the relaxation times is found to be negligible in the calculation of $R_{\parallel}$, but is probably important for $R_{\perp}$. As temperature increases, the changing c/a ratio and decreasing band gaps, as affected by the Debye-Waller factor, combine to reduce the values of the Hall constants. Our predictions for $R_{\parallel}$ and $R_{\perp}$ appear to agree quite satisfactorily with values extrapolated from measurements at lower temperatures.

We simplify the Fermi surface model further in our treatment of thermoelectric power. As in the noble metals, the shape of the form factor results in a positive contribution. Anisotropy in our calculated values of S_a and S_c is due primarily to distortion of the Fermi surface. Our predicted values appear reasonable in light of available experimental data at lower temperatures.

PART I

INTRODUCTION

A. Historical Review

1. General Transport Theory

The classical theory of electron transport in metals was developed by Drude[1] and Lorentz[2] in terms of a relaxation time that represented the mean time between collisions. Sommerfeld[3] reformulated the problem in a quantum mechanical framework. He used Fermi-Dirac statistics for the electrons, but he retained the concept of a simple relaxation time to describe the effect of collision processes.

More recent transport theory has been based upon the linearized Boltzmann equation[4] (Eq. 1.1), which describes the balance at steady state between the effects of the applied electric field $\vec{E}$ and conduction electron scattering,

$$-\left(\frac{\partial f^0}{\partial \epsilon}\right)\vec{v}(\vec{k})\cdot e\vec{E} = \int\left[g(\vec{k})-g(\vec{k}')\right]W(\vec{k},\vec{k}')d^3k' \quad . \tag{1.1}$$

Here $g(\vec{k})$ represents the steady state deviation of the electron distribution from the the Fermi-Dirac function, f^0. $W(\vec{k},\vec{k}')$ is proportional to the transition probability from state $\vec{k}$ to $\vec{k}'$, and ϵ and $\vec{v}$ are the electron energy and velocity. The relaxation time approximation consists of taking the function $g(\vec{k})$ to be of the form

$$g(\vec{k}) = -\left(\frac{\partial f^0}{\partial \epsilon}\right)e\vec{E}\cdot\tau\vec{v}(\vec{k}) \quad , \tag{1.2}$$

where again $\vec{v}(\vec{k})$ is the electron velocity. In the case of free electrons; i.e., for a spherical Fermi surface and $W(\vec{k},\vec{k}')$ depending only on $|\vec{k}-\vec{k}'|$, it can rigorously be shown[5] that a constant relaxation time exists in

the form

$$\frac{1}{\tau} = \int_{\text{Fermi Surface}} \left[1-\cos\Theta(\vec{k},\vec{k}')\right] W(\vec{k},\vec{k}') \frac{dS'}{\hbar v'} \quad . \tag{1.3}$$

This model satisfactorily describes the resistivity of the monovalent metals, but does rather poorly with the multivalents. Obviously, it cannot hope to deal with anisotropies in non-cubic systems, the problem to which the present work is directed.

Several workers have attempted to modify Eq. (1.3) in some physically reasonable way.[6-11] For example, Giaever[10] used Eq. (1.3) to define a $\vec{k}$-dependent "relaxation time." Truant and Carbotte[11] later used the same formula to calculate a relaxation time for Zn, ignoring the anisotropic structure of the material. Such approximations met with limited success, but they can result in considerable error, even in the relatively simple noble metal systems.[12]

One possible approach is to avoid the direct solution of Eq. (1.1), solving directly instead for the resistivity using a variational procedure.[13] This technique has been applied with varying degrees of success to many metals.[14-16] However, as pointed out by Robinson and Dow,[17] variational ratios (e.g. for the resistivity) which explicitly take anisotropy into account do not simplify sufficiently to appear advantageous. Also, the presence of anisotropy significantly increases the ambiguity and uncertainty inherent in the choice of trial functions.

A general method of attacking Eq. (1.1) is to define $g(\vec{k})$ in terms of a vector mean free path $\vec{\lambda}(\vec{k})$;[18] i.e.,

$$g(\vec{k}) = -\left(\frac{\partial f^0}{\partial \epsilon}\right) e\vec{E}\cdot\vec{\lambda}(\vec{k}) \quad . \tag{1.4}$$

Taylor[19] discussed the solution of Eq. (1.1) directly for the vector $\vec{\lambda}$. It is also possible to introduce a modified "relaxation time"[20] by the relation

$$\vec{\lambda}(\vec{k}) = \overline{\overline{\tau}}\,\vec{v}(\vec{k}) \tag{1.5}$$

where $\overline{\overline{\tau}}$ is in general a second rank tensor. The three independent quantities determined by the Boltzmann equation can be taken to be the diagonal components of $\overline{\overline{\tau}}$ referred to its principal axes. Chan and Huntington[21-22] used this approach, combined with a Nearly Free Electron Model (NFEM) based upon the pseudopotential concept[23-24] to investigate the conductivity anisotropy in single crystal Zn. The Chan, Huntington calculation explained how large elastic and Fermi surface anisotropies in Zn combine to result in a nearly isotropic conductivity tensor.[25-26] The success of this calculation suggested using a similar model to investigate other transport parameter anisotropies.

2. Driving Force for Electromigration

One of the transport phenomena sensitive to anisotropies in the metal system is the driving force for electromigration, or mass transport in a metal carrying a high electric current density. The force itself is derived from the measured drift velocity through the Nernst-Einstein relation, and is usually expressed in terms of an effective charge relating it to the applied electric field. The total force on the diffusing atom has two parts, the electrostatic force of the applied electric field, and the "electron-wind" force, due to collisions between the atom and the current-carrying electrons. We shall be dealing primarily with the second contribution, that due to the streaming charge carriers.

The early theories of Fiks[27] and Huntington and Grone[28] determine the wind force by calculating the momentum transfer by the electrons per unit time as they are scattered by the atom. Bosvieux and Friedel[29] noted that the electron current induces a dipolar-like distortion in the screening cloud associated with the diffusing atom, resulting in a net electrostatic force. Later, Sorbello[30] extended this viewpoint to a more realistic model of a metal within the framework of pseudopotential theory. A somewhat related transport-theory based screening calculation was performed by Das and Peierls.[31] More recently, a number of calculations[32-34] have been performed using Kubo's linear response formalism.[35] All of these viewpoints lead essentially to the same conclusions concerning the wind force in the FEM; i.e., that the force depends on the specific resistivity of the diffusing atom and on the number of electrons per atom.

In order to treat anisotropic effects realistically, the theory must be extended to include band structure effects. The first efforts in this direction were made by Fiks[36-37] and by Feit and Huntington.[38] In both of these theories, the diffusing atom was considered to be in an extended plane wave state, an assumption which appears to be more appropriate for a free particle; e.g., a neutron. In addition, neither treatment dealt with the complications arising from screening in a Bloch electron gas. No quantitative evaluations of band structure effects in electromigration have been published.

We are especially interested in the effective charge of Zn since it is one of the materials in which single crystal measurements[39] have been made. In this work, Routbort found that the driving force was

about half as effective along the hexagonal axis as perpendicular to it. In light of the nearly isotropic conductivity of Zn, these results were initially puzzling,[38] which stimulated the work of Chan and Huntington[22] as well as the present work.

3. Hall Effect

The transport properties of a solid may be profoundly altered by the application of a magnetic field. Analysis of these effects requires inclusion of an additional term in the Boltzmann equation for the distribution function $g(\vec{k})$ (see PART III). In the relaxation time approximation, Jones and Zener[40] proposed a solution for $g(\vec{k})$ as an expansion in powers of the magnetic field $\vec{H}$. In the weak field limit, the resulting expression for the Hall coefficient in cubic materials is quite sensitive to the shape of the Fermi surface, involving the second derivatives of the electron energy (first derivatives of electron velocity) with respect to wavevector $\vec{k}$. Ziman[41] applied this model to a calculation of the Hall effect in the noble metals. Using what he called an "eight-cone model" to account for distortions of the Fermi surface from sphericity, he obtained quite satisfactory agreement with experiment.

Price[18] and Taylor[19] have shown how to extend the method of Jones and Zener to anisotropic materials in terms of the vector mean free path, $\vec{\lambda}$. In this case, the Hall coefficient involves the derivatives of $\vec{\lambda}$ with respect to $\vec{k}$. Calculations using the above model have not yet been carried out for the hexagonal metals.

Experimental measurements of the Hall coefficients in Zn and Cd single crystals were made by Lare, et. al.[42] in 1964 and more recently

by Yonemitsu and Takahashi.[43] They reveal a large anisotropy and indicate the predominance of "hole-like" carriers, while both the a and c-axis values tend to decrease with increasing temperature. On the other hand, the electromigration experiments suggest "negative charge carriers"; thus, there is no clear, simple correlation between the electromigration results and the Hall constants.[39] Recent calculations by Cowley and Stringer[44] using the Plane Faced Energy Surface (PFES) method[45-46] achieved rough agreement with experimental values at room temperature.

4. Thermoelectric Power

The usual derivation of the expression for the thermoelectric power of a metal[47] is easily generalized to anisotropic metals (see PART IV) and gives the same result

$$S = \frac{\pi^2 k_B^2 T}{3e} \left[\frac{1}{\sigma(\epsilon)} \frac{\partial \sigma}{\partial \epsilon} \right]_{\epsilon = \epsilon_F} , \qquad (1.6)$$

where $\sigma(\epsilon)$ is the electrical conductivity of a metal whose Fermi energy is ϵ_F. Comparison of the theory with experiment is complicated by the effect of "phonon drag",[48] which, however, disappears at high temperatures and will be neglected here. Taking e as a negative quantity, one finds from the formula that a free-electron metal should have a negative thermopower. As is well known, however, the thermopower of Li as well as all three noble metals is positive in sign.

Ziman[41,49] attempted to resolve this paradox for the noble metals by considering the effect of Fermi surface distortion, but was unsuccessful. Taylor[12] later modified the model for Cu by including additional band structure effects, but succeeded only in driving his theoretical values farther away from the experimental values. A new

line of thought was suggested by Robinson,[50] and developed to account for the positive thermopower of Li.[17] It is that a critical determinant of transport properties in the simple metals is the shape of the form factor (Fourier transform of the effective scattering pseudopotential) resulting from interference between Coulomb attraction and core repulsion potentials. Subsequent calculations for the noble metals[51-53] have quantitatively verified Robinson's qualitative observations.

Measurements[54,55] for Zn and Cd also show positive values of the thermopower, as well as a large anisotropy between a and c-axis values. To date, however, no calculations, such as the above described work on the noble metals, have been carried out for anisotropic materials.

B. Introduction to the Problem

As pointed out recently by Hurd,[56] the study of low field galvanomagnetic effects in anisotropic metals is presently a somewhat neglected subject. Much of the existing data is either quite old or, in many cases, incomplete in terms of temperature dependence. On the theoretical side, complications arising from the anisotropic structure and from electron band effects have largely discouraged quantitative investigations. It is the aim of the work presented here to take a more comprehensive look into the transport properties of Zn than has heretofore been attempted.

The model used here for the Fermi surface and electron wavefunctions is consistent with that used by Chan and Huntington in their investigation of the high temperature conductivity. It is a 2-OPW model, similar to that employed by Ziman[41] for the noble metals, in which the effects of the most important Brillouin Zone discontinuities

are accounted for, one pair at a time. While this is a highly approximate model, and perhaps more appropriate for the simpler noble metals, we feel it retains the essential band structure effects in the hexagonal metals. In addition, we assume throughout the existence of a local pseudopotential form factor (see APPENDIX A) determined semi-empirically from a prescription given by Stark and Falicov.[57] In light of these and other approximations invoked during the course of the following calculations, the results presented here are not expected to produce exact agreement with experiment; in fact, high temperature measurements of the Hall effect and thermoelectric power are incomplete. Instead, we hope to present a consistent, semi-quantitative picture of the essential physical considerations resulting in transport parameter anisotropy.

PART II concerns the driving force for electromigration. First, the general theory of band structure effects in electromigration is reconsidered by combining, to a certain extent, the approaches of Feit[38] and Sorbello.[30] The effects of band structure on electron screening are explicitly taken into account using the "dielectric matrix" formalism.[58,59] Several simplifying approximations are made and model calculations are carried out for Zn. In PART III, the two independent Hall constants of Zn are calculated and compared with experiment. The temperature dependence of these coefficients is also analyzed in terms of changing Fermi surface-Brillouin Zone wall interactions. In PART IV, the anisotropy in thermoelectric power coefficients is calculated. Finally, a discussion of all the results presented in PARTS II-IV is given in PART V.

PART II

DRIVING FORCE FOR ELECTROMIGRATION

A. General Theory

The driving force on a diffusing ion in the presence of high electric current derives from two possible sources. The first is due to the electrostatic interaction of the ion with the external field and the second is due to the interaction with the charge carriers. In this treatment, we split the total effective charge, Z^*, into

$$Z^* = Z_e + Z_w \quad , \tag{2.1}$$

where Z_e is the effective electrostatic charge and Z_w is the momentum transfer or electron wind charge. (It should be pointed out that although this separation has been the starting point of most discussions of electromigration, it is not essential. Some recent investigators[32-34] have preferred to deal directly with the total driving force from first principles via a linear response formalism.) In the next section, we present a few remarks concerning Z_e, and then Z_w will be considered in detail.

1. Electrostatic Force

A controversial question in the theory concerns the extent to which the direct force of the applied field is screened by the conduction electron gas. In the models of Huntington[60] and others[31,61] there is no appreciable screening of the external field and the full electrostatic force ZeE, where Z is the ionic valence, is felt. On the other hand, Bosvieux and Friedel[29] maintain that for interstitial ions the direct field force is totally screened out. Recently, however,

Sham claims to have shown that the Bosvieux-Friedel argument is wrong, basing his results on a quantum field theoretic treatment of the problem. Landauer[62] argues that significant local screening may be present, tracing the source to what he calls "spatial conductivity modulation"[63] and "residual resistivity dipoles."[64,65] While it is generally conceded that the effects suggested by Landauer are real,[34,66] the magnitude of these effects remains uncertain. Bibby and Youdelis[67] attempted to answer the question experimentally, looking at the electromigration of carbon and nitrogen in the Hall field perpendicular to the current direction. These authors concluded that the full electrostatic force corresponding to the nominal ionic valence was present. A recent, as yet unpublished, communication[68] suggests that the controversy has not yet been fully resolved. Nevertheless, in comparing our calculations to experiment, we will subscribe to the view that the full electrostatic force is exerted by the external field.

2. Force on a Diffusing Atom in a Drifting Gas of Bloch Electrons

We calculate here the effects of the electric current on an atom diffusing in a crystal lattice. Let $\vec{R}$ represent the coordinate of the diffusing particle. From the relationship between a coordinate and its canonically conjugate momentum we write

$$\frac{d}{dt}\langle\vec{P}\rangle = -\left\langle\Psi\left|\frac{\partial H}{\partial \vec{R}}\right|\Psi\right\rangle \quad , \tag{2.2}$$

where Ψ represents the exact wavefunction of the system and H is the total Hamiltonian. We proceed now in the spirit of the Born-Oppenheimer approximation,[69] i.e., the migrating ion is considered to be a very heavy classical particle interacting with a quantum mechanical electron gas. At each point along its diffusion path, the ion is taken to be fixed in

position as it interacts with the electrons. For such a classical particle, we may identify $\frac{d\langle\vec{P}\rangle}{dt}$ as a force on the particle and write Eq. (2.2) as

$$\vec{F} = -\left\langle \Psi \left| \frac{\partial H}{\partial \vec{R}} \right| \Psi \right\rangle \quad . \tag{2.3}$$

We are interested only in the current dependent electron driving force on the ion, so in Eq. (2.3) we replace H by U, the electron defect interaction potential. (In the case of interstitial diffusion, U may be a single point ion potential. For diffusion by the vacancy mechanism, U must include the potential of the jumping ion as well as the "semi-vacancies" at either end of the diffusion path.)[38] Distortion of the lattice due to the presence of the defect will be neglected. Our starting point then is

$$\vec{F} = -\left\langle \Psi \left| \frac{\partial U}{\partial \vec{R}} \right| \Psi \right\rangle \quad . \tag{2.4}$$

If we separate Ψ into a product of electron and defect parts in which the positions of the ions are fixed, and take the electron wavefunction to be a product of one electron functions, we arrive at

$$\vec{F} = -\sum_{\vec{k}} f(\vec{k}) \left\langle \psi_{\vec{k}} \left| \frac{\partial U}{\partial \vec{R}} \right| \psi_{\vec{k}} \right\rangle \quad . \tag{2.5}$$

In Eq. (2.5), $f(\vec{k})$ represents the electron distribution function in the presence of the applied electric field. It of course must be perturbed from the Fermi-Dirac function f^0 in order to reflect the presence of current. In what follows, we will assume that $f(\vec{k})$ is a known function, having been determined from an independent solution of the Boltzmann equation in the high temperature range. In our numerical computations, the actual solution of Chan and Huntington[22] for the electron mean free path $\vec{\lambda}$ (see APPENDIX C) will be used.

For an isolated interstitial, take U to be of the form $u(\vec{r}-\vec{R})$, $\vec{r}$ being the electron coordinate, $\vec{R}$ the coordinate of the diffusing ion, keeping in mind that u denotes an unscreened potential. (In the case of diffusion by the vacancy mechanism, we would take

$$U = u(\vec{r}-\vec{R}) - u(\vec{r}-\vec{R}_1) - u(\vec{r}-\vec{R}_2) \quad , \tag{2.6}$$

$\vec{R}_1$ and $\vec{R}_2$ denoting the positions of the semi-vacancies. We will return to this point later.) Fourier expand u as follows:

$$u(\vec{r}-\vec{R}) = \sum_{\vec{q}} u(\vec{q}) e^{i\vec{q}\cdot(\vec{r}-\vec{R})} \quad , \tag{2.7a}$$

where

$$u(\vec{q}) = \frac{1}{\Omega}\int u(\vec{x}) e^{-i\vec{q}\cdot\vec{x}} d\vec{x} \quad . \tag{2.7b}$$

(Ω is the crystal volume.) Using Eq. (2.7), we arrive at

$$\frac{\partial U}{\partial \vec{R}} = -i \sum_{\vec{q}} \vec{q}\, u(\vec{q}) e^{i\vec{q}\cdot(\vec{r}-\vec{R})} \quad . \tag{2.8}$$

Note that Eq. (2.8) is valid in either the vacancy or interstitial case. Substituting in Eq. (2.5) gives

$$\vec{F} = \sum_{\vec{k}} \sum_{\vec{q}} f(\vec{k}) i\vec{q}\, u(\vec{q}) e^{-i\vec{q}\cdot\vec{R}} \left\langle \psi_{\vec{k}} \middle| e^{i\vec{q}\cdot\vec{r}} \middle| \psi_{\vec{k}} \right\rangle \quad . \tag{2.9}$$

We now have to calculate the one-electron wavefunctions $\psi_{\vec{k}}$. At this point in his development, Feit[38] replaced U everywhere by a screened potential, screened as it would be in the absence of current in a free electron gas. He then calculated the electron wavefunctions ψ using perturbation theory, neglecting any other contributions to screening. We depart from that approach here and proceed as in Sorbello;[30] treating U as a bare unscreened potential in Eq. (2.5),

but accounting for the electron-electron interactions by calculating the ψ's self-consistently (in the Hartree approximation) to first order in the defect potential. Unlike the Sorbello treatment, we assume a weak, local potential for the ions, and treat the case of Bloch electrons. Our zero-order wavefunctions therefore will have a spatially varying part of the form

$$\phi_{\vec{k}}(\vec{r}) = \sum_{\vec{G}} a_{\vec{G}}(\vec{k}) e^{i(\vec{k}+\vec{G})\cdot\vec{r}} \quad , \tag{2.10}$$

where the sum is, in general, over the set of all reciprocal lattice vectors. Using first order scattering theory,[70] we can write the wavefunction $\psi_{\vec{k}}$ arising from the electron-defect interaction as

$$\psi_{\vec{k}} = |\phi_{\vec{k}}\rangle + \sum_{\vec{k}'} \frac{|\phi_{\vec{k}'}\rangle\langle\phi_{\vec{k}'}|W|\phi_{k}\rangle}{\epsilon(\vec{k}) - \epsilon(\vec{k}') + i\alpha} \quad . \tag{2.11}$$

In Eq. (2.11), the potential W must be self-consistently determined. The Bloch functions ϕ are the self-consistent eigenstates of the crystal lattice potential. W therefore includes the defect potential, as well as the change in the screening potential of the conduction electrons due to the presence of the defect. In order to determine the latter, we need an expression for the total conduction electron charge density, which may be written

$$n(\vec{r}) = \sum_{\vec{k}} f(\vec{k}) \psi^{*}_{\vec{k}} \psi_{\vec{k}} \quad . \tag{2.12}$$

Fourier transforming Eq. (2.12) gives

$$n(\vec{q}) = \frac{1}{\Omega} \int \sum_{\vec{k}} f(\vec{k}) \psi^{*}_{\vec{k}} \psi_{\vec{k}} e^{-i\vec{q}\cdot\vec{x}} d\vec{x} \quad . \tag{2.13}$$

We wish to obtain expressions in terms of the zero-order wavefunctions; accordingly, we use the relation

$$\langle\psi_{\vec{k}}| = \sum_{\vec{k}} \langle\psi_{\vec{k}}|\phi_{\vec{k}}\rangle\langle\phi_{\vec{k}}| \tag{2.14}$$

to rewrite Eq. (2.13) in the form

$$n(\vec{q}) = \frac{1}{\Omega} \sum_{\vec{k}} \sum_{\vec{k}'} f(\vec{k}) \langle \psi_{\vec{k}'} | \phi_{\vec{k}} \rangle \langle \phi_{\vec{k}'} | e^{-i\vec{q}\cdot\vec{r}} | \psi_{\vec{k}''} \rangle \quad . \tag{2.15}$$

Now, the perturbation expression in Eq. (2.11) can be used to evaluate the matrix elements in Eq. (2.15). The results are

$$\langle \psi_{\vec{k}'} | \phi_{\vec{k}} \rangle = \langle \phi_{\vec{k}'} | \phi_{\vec{k}} \rangle + \frac{\langle \phi_{\vec{k}'} | W | \phi_{\vec{k}} \rangle}{\epsilon(\vec{k}) - \epsilon(\vec{k}') - i\alpha} \tag{2.16}$$

and

$$\langle \phi_{\vec{k}} | e^{-i\vec{q}\cdot\vec{r}} | \psi_{\vec{k}''} \rangle = \langle \phi_{\vec{k}} | e^{-i\vec{q}\cdot\vec{r}} | \phi_{\vec{k}''} \rangle + \sum_{\vec{k}'''} \frac{\langle \phi_{\vec{k}} | e^{-i\vec{q}\cdot\vec{r}} | \phi_{\vec{k}'''} \rangle \langle \phi_{\vec{k}'''} | W | \phi_{\vec{k}''} \rangle}{\epsilon(\vec{k}) - \epsilon(\vec{k}''') + i\alpha} \quad , \tag{2.17}$$

where the orthogonality of the Bloch functions ($\langle \phi_{\vec{k}'} | \phi_{\vec{k}} \rangle = \delta(\vec{k}-\vec{k}')$) has been used. With Eqs. (2.16) and (2.17), Eq. (2.15) becomes

$$n(\vec{q}) = \frac{1}{\Omega} \sum_{\vec{k}} f(\vec{k}) \langle \phi_{\vec{k}} | e^{-i\vec{q}\cdot\vec{r}} | \phi_{\vec{k}} \rangle + \frac{1}{\Omega} \sum_{\vec{k},\vec{k}'} f(\vec{k}) \frac{\langle \phi_{\vec{k}} | e^{-i\vec{q}\cdot\vec{r}} | \phi_{\vec{k}'} \rangle \langle \phi_{\vec{k}'} | W | \phi_{\vec{k}} \rangle}{\epsilon(\vec{k}) - \epsilon(\vec{k}') - i\alpha}$$

$$- \frac{1}{\Omega} \sum_{\vec{k},\vec{k}'} f(\vec{k}) \frac{\langle \phi_{k} | e^{-iq\cdot r} | \phi_{\vec{k}'} \rangle \langle \phi_{\vec{k}'} | W | \phi_{k} \rangle}{\epsilon(k) - \epsilon(\vec{k}') + i\alpha} \quad . \tag{2.18}$$

The first term on the right side of Eq. (2.18) represents the zero-order charge density; i.e., the charge density in the absence of the impurity, depending only on the Bloch wavefunctions ϕ. We need an expression for the change in charge density due to the presence of the defect, which comes from the remaining two terms. Calling this charge density Δn, we get from Eq. (2.18) the expression

$$\Delta n(\vec{q}) = \frac{1}{\Omega}\sum_{\vec{k},\vec{k}'} \langle \phi_{\vec{k}} | e^{-i\vec{q}\cdot\vec{r}} | \phi_{\vec{k}'} \rangle \langle \phi_{\vec{k}'} | W | \phi_{\vec{k}} \rangle \frac{f(\vec{k}') - f(\vec{k})}{\epsilon(\vec{k}) - \epsilon(\vec{k}') - i\alpha} \cdot \quad (2.19)$$

The function $f(\vec{k})$ may be split into two parts as discussed in PART I; i.e.,

$$f(\vec{k}) = f^0(\vec{k}) + g(\vec{k}) \quad (2.20)$$

where f^0 is the Fermi distribution function and $g(\vec{k})$ is the change giving rise to the current. Making use of Eq. (2.20) and the following relations:

$$f^0(\vec{k}) = f^0(-\vec{k}) ,$$

$$\epsilon(\vec{k}) = \epsilon(-\vec{k}) ,$$

$$g(\vec{k}) = -g(-\vec{k}) ,$$

$$\phi^*_{\vec{k}} = \phi_{-\vec{k}} ,$$

$$\frac{1}{\epsilon(\vec{k}) - \epsilon(\vec{k}') + i\alpha} = \frac{1}{\epsilon(\vec{k}) - \epsilon(\vec{k}')} - i\pi\delta\left[\epsilon(\vec{k}) - \epsilon(\vec{k}')\right] ,$$

Eq. (2.19) simplifies to

$$\Delta n(\vec{q}) = \frac{1}{\Omega}\sum_{\vec{k},\vec{k}'} \langle \phi_{\vec{k}} | e^{-i\vec{q}\cdot\vec{r}} | \phi_{\vec{k}'} \rangle \langle \phi_{\vec{k}'} | W | \phi_{\vec{k}} \rangle$$

$$\cdot \left\{ \frac{2f^0(\vec{k})}{\epsilon(\vec{k}) - \epsilon(\vec{k}')} - 2i\pi g(\vec{k})\delta\left[\epsilon(\vec{k}) - \epsilon(\vec{k}')\right] \right\} \cdot \quad (2.21)$$

Next we explicitly divide the potential W into two parts,

$$W = U + \Delta V_s , \quad (2.22)$$

where ΔV_s means the change in the screening potential due to the defect. ΔV_s can be further broken up into $\Delta V_s^0 + \Delta V_s^c$, where the superscript 0 denotes that part of ΔV_s independent of the current, and ΔV_s^c is the

current dependent part. With this notation,

$$W = U + \Delta V_s^0 + \Delta V_s^c \quad . \tag{2.23}$$

Now write

$$W^0 = U + \Delta V_s^0 \tag{2.24}$$

so that W^0 represents the defect potential screened as it would be in the zero current case. (It will be instructive to write some of our expressions in terms of this potential, which we may assume to be known from the solution of the zero-order problem.)

Before proceeding, we can perform an intermediate check by comparing Eq. (2.21) with an expression derived by Stoddart, et. al.[71] by an alternate formalism. They considered the charge distribution around a weak scattering impurity in a stationary gas of Bloch electrons. From Eq. (2.20), we get for the change in charge density in the zero current case

$$\Delta n^0(\vec{q}) = \frac{1}{\Omega} \sum_{\vec{k},\vec{k}'} \langle \phi_{\vec{k}} | e^{-i\vec{q}\cdot\vec{r}} | \phi_{\vec{k}'} \rangle \langle \phi_{\vec{k}'} | W^0 | \phi_{\vec{k}} \rangle \frac{2f^0(\vec{k})}{\epsilon(\vec{k}) - \epsilon(\vec{k}')} \quad , \tag{2.25}$$

which agrees with their equation (3.10).

Poisson's equation (transformed) can now be used to relate Δn and ΔV_s. Specifically,

$$\Delta V_s(\vec{q}) = \frac{4\pi e^2}{q^2} \Delta n(\vec{q}) \quad . \tag{2.26}$$

By combining Eqs. (2.26) and (2.21), we arrive at the following expression for $\Delta V_s(\vec{q})$:

$$\Delta V_s(\vec{q}) = \frac{4\pi e^2}{q^2 \Omega} \sum_{\vec{k},\vec{k}'} \langle \phi_{\vec{k}} | e^{-i\vec{q}\cdot\vec{r}} | \phi_{\vec{k}'} \rangle \langle \phi_{\vec{k}'} | W | \phi_{\vec{k}} \rangle \frac{2f^0(\vec{k})}{\epsilon(\vec{k}) - \epsilon(\vec{k}')}$$

$$- \frac{i8\pi^2 e^2}{q^2 \Omega} \sum_{\vec{k},\vec{k}'} \langle \phi_{\vec{k}} | e^{-i\vec{q}\cdot\vec{r}} | \phi_{\vec{k}'} \rangle \langle \phi_{\vec{k}'} | W^0 | \phi_{\vec{k}} \rangle g(\vec{k}) \delta \left[\epsilon(\vec{k}) - \epsilon(\vec{k}') \right] . \quad (2.27)$$

(In the second term on the right of Eq. (2.27), W^0 rather than W appears since the term involving ΔV_s^c and $g(\vec{k})$ contains the product of two small quantities.) From Eq. (2.27) we can write

$$\Delta V_s^0(\vec{q}) = W^0(\vec{q}) - U(\vec{q})$$

$$= \frac{4\pi e^2}{q^2 \Omega} \sum_{\vec{k},\vec{k}'} \langle \phi_{\vec{k}} | e^{-i\vec{q}\cdot\vec{r}} | \phi_{\vec{k}'} \rangle \langle \phi_{\vec{k}'} | W^0 | \phi_{\vec{k}} \rangle \frac{2f^0(\vec{k})}{\epsilon(\vec{k}) - \epsilon(\vec{k}')} \quad (2.28)$$

Eq. (2.28) relates the unscreened defect potential U to the defect potential screened in the zero current case (W^0). After considerable algebra, Eq. (2.28) can be generalized as follows:

$$\begin{bmatrix} \cdot \\ \cdot \\ \cdot \\ U(\vec{q}-\vec{G}) \\ U(\vec{q}) \\ U(\vec{q}+\vec{G}) \\ \cdot \\ \cdot \\ \cdot \end{bmatrix} = \begin{bmatrix} & & \\ & \approx\approx & \\ & \epsilon & \\ & & \end{bmatrix} \begin{bmatrix} \cdot \\ \cdot \\ \cdot \\ W^0(\vec{q}-\vec{G}) \\ W^0(\vec{q}) \\ W^0(\vec{q}+\vec{G}) \\ \cdot \\ \cdot \\ \cdot \end{bmatrix} \quad (2.29)$$

$\approx\approx\epsilon$ here can be interpreted as a "dielectric matrix" in analogy with the free electron dielectric function $\epsilon(\vec{q})$. Its rows and columns are labeled by reciprocal lattice vectors and its elements are given by

$$\epsilon(\vec{q}+\vec{G},\vec{q}+\vec{H}) = \delta_{\vec{G},\vec{H}} - \frac{4\pi e^2}{\Omega |\vec{q}+\vec{G}|^2} \sum_{\vec{k},\vec{L}} \frac{2f^0(\vec{k})}{\epsilon(\vec{k}) - \epsilon(\vec{k}+\vec{q}+\vec{L})}$$

$$\cdot \langle \phi_{\vec{k}} | e^{-i(\vec{q}+\vec{G})\cdot\vec{r}} | \phi_{\vec{k}+\vec{q}+\vec{L}} \rangle \langle \phi_{\vec{k}+\vec{q}+\vec{L}} | e^{i(\vec{q}+\vec{H})\cdot\vec{r}} | \phi_{\vec{k}} \rangle \quad (2.30)$$

where $\vec{L}$, $\vec{G}$, and $\vec{H}$ are reciprocal lattice vectors. In Eq. (2.30), we have used the notation of Sham and Ziman.[72] In this notation, Eq. (2.29) becomes

$$U(\vec{q}) = \sum_{\vec{G}} \epsilon(\vec{q},\vec{q}+\vec{G}) W^0(\vec{q}+\vec{G}) \quad . \tag{2.29a}$$

For notational simplicity, we write Eq. (2.29) in matrix-vector form:

$$\tilde{U}(\vec{q}) = \tilde{\tilde{\epsilon}}\,\tilde{W}^0(\vec{q}) \quad . \tag{2.31}$$

In this form, Eq. (2.31) formally resembles the scalar equation $U(\vec{q}) = \epsilon(\vec{q})W^0(\vec{q})$ which relates the screened and unscreened potentials in the free electron case.[73] The relationship between these potentials in the presence of the crystal lattice (Bloch electrons) is, of course, much more complicated.

In order to proceed, we assume that Eqs. (2.29) can be inverted and solved for the potentials $W^0(\vec{q}+\vec{G})$, and formally write

$$\tilde{W}^0(\vec{q}) = \tilde{\tilde{\epsilon}}^{-1}\tilde{U}(\vec{q}) \quad . \tag{2.32}$$

To further simplify the later discussion, note that $\tilde{\tilde{\epsilon}}$ may be written as follows:

$$\tilde{\tilde{\epsilon}} = \tilde{\tilde{I}} - \tilde{\tilde{D}}\tilde{\tilde{A}} \quad , \tag{2.33}$$

where $\tilde{\tilde{I}}$ is the identity matrix, and $\tilde{\tilde{D}}$ is a diagonal matrix whose elements are given by

$$D(\vec{q}+\vec{G},\vec{q}+\vec{G}) = \frac{4\pi e^2}{\Omega|\vec{q}+\vec{G}|^2} \quad . \tag{2.34}$$

The elements of $\tilde{\tilde{A}}$ follow from Eq. (2.30). We now need an expression for $\Delta V_s^c(\vec{q})$, which we get from Eq. (2.27):

$$\Delta V_s^c(\vec{q}) = \frac{4\pi e^2}{q^2\Omega}\sum_{\vec{k},\vec{k}'}\langle\phi_{\vec{k}}|e^{-i\vec{q}\cdot\vec{r}}|\phi_{\vec{k}'}\rangle\langle\phi_{\vec{k}'}|\Delta V_s^c|\phi_{\vec{k}}\rangle\frac{2f^0(\vec{k})}{\epsilon(\vec{k}) - \epsilon(\vec{k}')}$$

$$-\frac{i8\pi^2e^2}{q^2\Omega}\sum_{\vec{k},\vec{k}'}\langle\phi_{\vec{k}}|e^{-i\vec{q}\cdot\vec{r}}|\phi_{\vec{k}'}\rangle\langle\phi_{\vec{k}'}|W^0|\phi_{\vec{k}}\rangle g(\vec{k})\delta\left[\epsilon(\vec{k})-\epsilon(\vec{k})\right] \quad . \qquad (2.35)$$

Writing Eq. (2.35) in matrix form in analogy with Eq. (2.29), and using Eq. (2.33), gives:

$$\widetilde{\Delta V}_s^c(\vec{q}) = \tilde{\tilde{D}}\tilde{\tilde{A}}\,\widetilde{\Delta V}_s^c(\vec{q}) - 2\pi i\,\tilde{\tilde{D}}\tilde{\tilde{B}}\,\tilde{W}^0(\vec{q}) \qquad (2.36)$$

or

$$\widetilde{\Delta V}_s^c(\vec{q}) = -2\pi i\,\tilde{\tilde{\epsilon}}^{-1}\tilde{\tilde{D}}\tilde{\tilde{B}}\,\tilde{W}^0(\vec{q}) \quad , \qquad (2.37)$$

where the matrix $\tilde{\tilde{B}}$ is given by

$$B(\vec{q}+\vec{G},\vec{q}+\vec{H}) = \sum_{\vec{k},\vec{L}} g(\vec{k})\delta\left[\epsilon(\vec{k})-\epsilon(\vec{k}+\vec{q}+\vec{L})\right]\langle\phi_{\vec{k}}|e^{-i(\vec{q}+\vec{G})\cdot\vec{r}}|\phi_{\vec{k}+\vec{q}+\vec{L}}\rangle \cdot\langle\phi_{\vec{k}+\vec{q}+\vec{L}}|e^{i(\vec{q}+\vec{H})\cdot\vec{r}}|\phi_{\vec{k}}\rangle \quad . \qquad (2.38)$$

Eq. (2.37) is the central result of this section; it represents the distortion of the screening cloud around the defect in the presence of the current. It is straightforward to show that in the free electron limit, Eq. (2.37) goes over into

$$\Delta V_s^c(\vec{q}) \underset{(FE)}{=} \frac{-2\pi i}{\epsilon(\vec{q})}\frac{4\pi e^2}{q^2\Omega}W^0(\vec{q})\sum_{\vec{k}} g(\vec{k})\delta\left[\epsilon(\vec{k})-\epsilon(\vec{k}+\vec{q})\right] \quad , \qquad (2.39)$$

which agrees with the expression derived by Sorbello.[74]

We are now ready to return to the expression for the force, Eq. (2.9), substituting the results of the screening calculation. First, rewrite Eq. (2.9) replacing $\vec{q}$ by $-\vec{q}$ in the summation:

$$\vec{F} = \sum_{\vec{q}} -i\vec{q}\,u^*(\vec{q})e^{i\vec{q}\cdot\vec{R}}\sum_{\vec{k}} f(\vec{k})\langle\psi_{\vec{k}}|e^{-i\vec{q}\cdot\vec{r}}|\psi_{\vec{k}}\rangle \quad . \qquad (2.40)$$

The sum over $\vec{k}$ in Eq. (2.40) is just $\Omega n(q)$, which was written out in Eq. (2.18). The first term is just the charge density in the absence of the defect (arising from the unperturbed Bloch wavefunctions) and

is not of interest here. We also get a contribution from $\Delta n^0(\vec{q})$ which is just the change in charge density in the zero current case, evaluated in Eq. (2.25). This part of the force is not of interest either; we want the current dependent part. This must come from the current dependent change in the charge density, which we can get from Eq. (2.37):

$$\Delta n^c(\vec{q}) = \frac{q^2\Omega}{4\pi e^2}\Delta V_s^c(\vec{q})$$

$$= -\frac{2\pi i q^2\Omega}{4\pi e^2}\sum_{\vec{K},\vec{L},\vec{M}} \epsilon^{-1}(\vec{q},\vec{q}+\vec{K})D(\vec{q}+\vec{K},\vec{q}+\vec{L})B(\vec{q}+\vec{L},\vec{q}+\vec{M})W^0(\vec{q}+\vec{M})$$

$$= -2\pi i\sum_{\vec{L},\vec{M}} \frac{q^2}{|\vec{q}+\vec{L}|^2}\epsilon^{-1}(\vec{q},\vec{q}+\vec{L})B(\vec{q}+\vec{L},\vec{q}+\vec{M})W^0(\vec{q}+\vec{M}) \quad . \qquad (2.41)$$

$W^0(\vec{q}+\vec{M})$ may be expressed in terms of the unscreened potential as follows:

$$W^0(\vec{q}+\vec{M}) = \sum_{\vec{G}} \epsilon^{-1}(\vec{q}+\vec{M},\vec{q}+\vec{G})U(\vec{q}+\vec{G}) \qquad (2.42)$$

Also we note that

$$-\frac{q^2}{|\vec{q}+\vec{L}|^2}\epsilon(\vec{q},\vec{q}+\vec{L}) = \epsilon^*(\vec{q}+\vec{L},\vec{q}) \qquad (2.43)$$

which follows from the definition in Eq. (2.30). Eq. (2.43) implies that the same property holds true for $\tilde{\tilde{\epsilon}}^{-1}$, which is proved as follows:

$$\sum_{\vec{G}} \epsilon(\vec{q}+\vec{M},\vec{q}+\vec{G})\,\epsilon^{-1}(\vec{q}+\vec{G},\vec{q}+\vec{L}) = \delta_{\vec{M},\vec{L}}$$

$$\Rightarrow \sum_{\vec{G}} \frac{|\vec{q}+\vec{G}|^2}{|\vec{q}+\vec{M}|^2}\epsilon^*(\vec{q}+\vec{G},\vec{q}+\vec{M})\,\epsilon^{-1}(\vec{q}+\vec{G},\vec{q}+\vec{L}) = \delta_{\vec{M},\vec{L}}$$

$$\Rightarrow \sum_{\vec{G}} |\vec{q}+\vec{G}|^2\,\epsilon^*(\vec{q}+\vec{G},\vec{q}+\vec{M})\,\epsilon^{-1*}(\vec{q}+\vec{M},\vec{q})\,\epsilon^{-1}(\vec{q}+\vec{G},\vec{q}+\vec{L})$$

$$= \delta_{\vec{M},\vec{L}}\,|\vec{q}+\vec{M}|^2\,\epsilon^{-1*}(\vec{q}+\vec{M},\vec{q})$$

Summing both sides over $\vec{M}$ gives

$$|\vec{q}|^2 \epsilon^{-1}(\vec{q},\vec{q}+\vec{L}) = |\vec{q}+\vec{L}|^2 \epsilon^{-1*}(\vec{q}+\vec{L},\vec{q}) \tag{2.44}$$

Using Eqs. (2.42) and (2.44) in (2.41) yields

$$\Delta n^c(\vec{q}) = -2\pi i \sum_{\vec{G},\vec{L},\vec{M}} B(\vec{q}+\vec{L},\vec{q}+\vec{M})\, \epsilon^{-1*}(\vec{q}+\vec{L},\vec{q})\, \epsilon^{-1}(\vec{q}+\vec{M},\vec{q}+\vec{G}) U(\vec{q}+\vec{G}) \tag{2.45}$$

Now Eq. (2.45) may be substituted in Eq. (2.40) to give the complete expression for the current dependent force:

$$\vec{F} = -2\pi \sum_{\vec{q}} \vec{q} e^{i\vec{q}\cdot\vec{R}} \sum_{\vec{G},\vec{L},\vec{M}} B(\vec{q}+\vec{L},\vec{q}+\vec{M})\, \epsilon^{-1}(\vec{q}+\vec{M},\vec{q}+\vec{G}) U(\vec{q}+\vec{G})\, \epsilon^{-1*}(\vec{q}+\vec{L},\vec{q}) u^*(\vec{q}) \quad . \tag{2.46}$$

Eq. (2.46) can be made more explicit by substituting for $\tilde{B}$ from its definition. Also, we can make the complete $\vec{R}$ dependence of the expression explicit by substituting for $U(\vec{q}+\vec{G})$, the defect potential. In our later computations, we will be interested in self-diffusion in Zn single crystals (via the vacancy mechanism). Therefore, for $U(\vec{q}+\vec{G})$ we use

$$U(\vec{q}+\vec{G}) = u(\vec{q}+\vec{G})\left[e^{-i(\vec{q}+\vec{G})\cdot\vec{R}} - e^{-i(\vec{q}+\vec{G})\cdot\vec{R}_1} - e^{-i(\vec{q}+\vec{G})\cdot\vec{R}_2}\right] , \tag{2.47}$$

which follows from Eqs. (2.6) and (2.7). Making these two substitutions in Eq. (2.46) results in

$$\vec{F} = -\frac{2\pi}{\hbar} \sum_{\vec{k},\vec{k}'} g(\vec{k})\delta\left[\epsilon(\vec{k})-\epsilon(\vec{k}')\right] \sum_{\vec{q}} \hbar\vec{q} \sum_{\vec{G},\vec{L},\vec{M}} \langle \phi_{\vec{k}'} | e^{-i(\vec{q}+\vec{L})\cdot\vec{r}} | \phi_{\vec{k}''} \rangle$$

$$\cdot \langle \phi_{\vec{k}''} | e^{i(\vec{q}+\vec{M})\cdot\vec{r}} | \phi_{\vec{k}} \rangle \epsilon^{-1}(\vec{q}+\vec{M},\vec{q}+\vec{G}) u(\vec{q}+\vec{G}) \epsilon^{-1*}(\vec{q}+\vec{L},\vec{q})$$

$$\cdot u^*(\vec{q}) S(\vec{q},\vec{G},\vec{R}) \quad , \tag{2.48}$$

where we have collected the $\vec{R}$ dependence of the expression into the term

$$S(\vec{q},\vec{G},\vec{R}) = e^{i\vec{q}\cdot\vec{R}}\left[e^{-i(\vec{q}+\vec{G})\cdot\vec{R}} - e^{-i(\vec{q}+\vec{G})\cdot\vec{R}_1} - e^{-i(\vec{q}+\vec{G})\cdot\vec{R}_2}\right] . \tag{2.49}$$

For purposes of comparison, it is instructive to consider the form of Eq. (2.48) in the free electron limit. Taking the matrix $\overleftrightarrow{\epsilon}$ over into the scalar function ϵ, and replacing the Bloch functions by plane waves we get

$$\vec{F}_{(FE)} = -\frac{2\pi}{\hbar}\sum_{\vec{k},\vec{k}'} g(\vec{k})\hbar(\vec{k}'-\vec{k})\left|w^0(\vec{k}'-\vec{k})\right|^2 S(\vec{k}'-\vec{k},\vec{0},\vec{R})\delta\left[\epsilon(\vec{k})-\epsilon(\vec{k}')\right]. \quad (2.50)$$

We take $g(\vec{k})$ from Eq. (1.2), τ having been determined from solving the Boltzmann equation. Eq. (2.50) is apparently the sum of momentum transfers $\hbar(\vec{k}-\vec{k}')$ for transitions between states on the Fermi surface, multiplied by the corresponding "Golden Rule" transition probability, calculated using a screened potential $w^0 = u/\epsilon$. For an isolated point defect, it would be exactly that. For the vacancy case, the formula is complicated by the appearance of the factor S, which accounts for the more complex defect structure involved in vacancy diffusion.

Eq. (2.48), however, is not subject to such a simple interpretation. Self-consistent screening of the potentials in the Bloch electron gas is accounted for formally by the appearance of elements of the inverse dielectric matrix. In simple terms, the screening cloud surrounding the diffusing particle is distorted by the presence of the lattice, even the zero current case, its distortion depending on the position $\vec{R}$ of the particle relative to the perfect lattice. This last point is worth some discussion, since in expressions such as Eq. (2.29a), the $\vec{R}$ dependence of the screening is not explicit, and perhaps not clear. (Assume for the moment an isolated point defect to simplify the writing.) Recalling Eq. (2.7), Eq. (2.29a) becomes

$$u(\vec{q})e^{-i\vec{q}\cdot\vec{R}} = \sum_{\vec{G}} \epsilon(\vec{q},\vec{q}+\vec{G})w^0(\vec{q}+\vec{G})e^{-i(\vec{q}+\vec{G})\cdot\vec{R}} \quad , \quad (2.51)$$

and the $\vec{R}$ dependence of the screening is explicit. Another point of possible confusion remains. The phase factors in Eq. (2.51) appear to depend on the choice of origin, which should otherwise be arbitrary. However, from Eq. (2.30), the elements of $\tilde{\tilde{\epsilon}}$ also depend on choice of origin implicitly through the Bloch wavefunctions ϕ. In fact, starting from Eq. (2.10), it is easily shown that a change of origin introduces an exactly compensating phase factor in the elements of $\tilde{\tilde{\epsilon}}$. Once the origin of coordinates is fixed, this arbitrariness in phase is removed from the elements of $\tilde{\tilde{\epsilon}}$ and $\tilde{\tilde{\epsilon}}^{-1}$, and simultaneously from Eq. (2.51).

The factor $-\hbar\vec{q}$ in Eq. (2.48) also deserves some comment. It apparently plays a role analogous to $\hbar(\vec{k}-\vec{k}')$, or momentum transfer, in the free electron case (Eq. (2.50)). From the form of the matrix elements in Eq. (2.48), we see that in the summation $\vec{q}$ is restricted to take on values of the form

$$\vec{q} = \vec{k}' - \vec{k} + \vec{N} \quad , \tag{2.52}$$

where $\vec{N}$ is a reciprocal lattice vector. In terms of plane waves, this is suggestive of simultaneous scattering by the defect and Bragg reflection by the crystal lattice, resulting in a momentum transfer $\hbar(\vec{k}-\vec{k}'-\vec{N})$. Strictly speaking, however, we know that the electron wind force cannot be analyzed exactly in terms of momentum transfer on a per collision basis, since the Bloch wavefunctions are not momentum eigenstates.

B. Application to Zinc

1. The NFE Model

In applying Eq. (2.48), by far the most serious complications arise in attempting to calculate $\tilde{\tilde{\epsilon}}$ and $\tilde{\tilde{\epsilon}}^{-1}$. Each element of $\tilde{\tilde{\epsilon}}$ involves

sums over the Bloch states and energies as given by Eq. (2.30), and $\tilde{\tilde{\epsilon}}$ has been the topic of considerable general discussion in the literature.[75] Little attention has been paid to actual numerical computations, particularly of off-diagonal terms. Some approximate calculations relevant to insulators and semiconductors are discussed by Sinha[76] in his review article. For metals, directional effects in screening have been largely ignored. In applying our NFE model to Zn, we will follow the latter course and replace $\tilde{\tilde{\epsilon}}$ with the free electron scalar form. We will, however, account for the Bloch nature of the zero-order states explicit in the matrix elements in Eq. (2.48) with a 2-OPW model. We should warn that the consistency of this procedure is not clear; the directional effects being ignored are not estimable in any obvious way. Arguments that they are small for a NFE metal would seem to apply equally well to the band structure effects being retained. We will see that those which are included in the computations do affect the quantitative results without significantly altering the overall qualitative picture.

In Eq. (2.48), the above approximation results in the expression

$$\vec{F} = -2\pi \sum_{\vec{k},\vec{k}'} g(\vec{k})\delta\left[\epsilon(\vec{k}) - \epsilon(\vec{k}')\right] \sum_{\vec{q}} \vec{q} \sum_{\vec{M}} \langle \phi_{\vec{k}'} | e^{-i\vec{q}\cdot\vec{r}} | \phi_{\vec{k}} \rangle \cdot \langle \phi_{\vec{k}} | e^{i(\vec{q}+\vec{M})\cdot\vec{r}} | \phi_{\vec{k}'} \rangle w^0(\vec{q}+\vec{M}) w^{0*}(\vec{q}) S(\vec{q},\vec{M},\vec{R}) \quad , \qquad (2.53)$$

w^0 being a screened potential ($w^0 = u/\epsilon$). This formula is similar to those derived by Feit[38] and Fiks;[37] except that it contains "cross terms" of the form $w^0(\vec{q}+\vec{M})w^{0*}(\vec{q})$, $\vec{M} \neq \vec{0}$. Such terms were absent from the above mentioned formulas because the authors both assumed a plane wave state for the diffusing particle, resulting in a sort of "pseudomomentum

conservation" condition. As pointed out earlier, the diffusing atom is treated here as a heavy, classical particle. The inclusion of quantum effects in the diffusion process is beyond the scope of this treatment.

In APPENDIX A, we describe the semi-empirical form factor F(q) which will be substituted for the spherically symmetric ionic potential w^0 in Eq. (2.53). F(q) will also be used to construct our Fermi surface model (see APPENDIX B), approximated by considering distortions arising from one pair of Brillouin zone walls at a time. The two plane wave wavefunctions consistent with this model have the standard form

$$\phi_{\vec{k}} = \alpha(\mu)e^{i\vec{k}\cdot\vec{r}} + \beta(\mu)e^{i(\vec{k}+\vec{K})\cdot\vec{r}} \quad , \tag{2.54}$$

where α and β are given by

$$\alpha(\mu) = \frac{1}{2}\left[1 + |\gamma-\mu|/\sqrt{(\gamma-\mu)^2 + g^2}\right]^{1/2} \quad , \tag{2.55a}$$

$$\beta(\mu) = \pm\frac{1}{2}\left[1 - |\gamma-\mu|/\sqrt{(\gamma-\mu)^2 + g^2}\right]^{1/2} \quad , \tag{2.55b}$$

and g is the parameter which determines the band gap splitting (see APPENDIX B). In Eqs. (2.55), $\gamma=K/2k_F$ and $\mu=k_{||}/k_F$ as in Fig. B.2. The sign of β is the same as F(K) for $\mu>\gamma$ and reverses for $\mu<\gamma$. This form for the wavefunctions allows explicit evaluation of the matrix elements in Eq. (2.53).

In APPENDIX C, the Chan, Huntington solution of the Boltzmann equation is briefly discussed and their findings are summarized. We take

$$g(\vec{k}) = e\vec{E}\cdot\vec{\lambda}(\vec{k})\delta[\epsilon(\vec{k})-\epsilon_F] \quad , \tag{2.56}$$

where

$$\lambda_{a,c} = \tau_{a,c}(\vec{k})\, v_{a,c}(\vec{k}) \quad , \tag{2.57}$$

the subscripts referring to the direction of the applied electric field, either in the basal plane (a) or along the hexagonal axis (c). The $\vec{k}$ dependence of τ in Eq. (2.57) turns out to be weak (see Fig. C.2); therefore, we replace $\tau_{a,c}(\vec{k})$ by the appropriate average also displayed in Fig. C.2. This was the procedure followed by Chan and Huntington in their conductivity calculations. The relevant numerical values are $\langle\tau_a\rangle = .47 \times 10^{-14}$ sec. and $\langle\tau_c\rangle = .28 \times 10^{-14}$ sec. The $\vec{k}$ dependence of the velocity factor in Eq. (2.57) is included as prescribed by our 2-OPW model of the Fermi surface. From APPENDIX B, we have

$$v_{\parallel}(\mu) \simeq \frac{\hbar k_F \mu}{m}\left[1 - 2\beta^2(\mu)\right]$$

and

$$v_{\perp}(\mu) = \frac{\hbar k_F \rho}{m} \quad ,$$

where the subscripts relate to the reciprocal lattice vector which defines the axis of cylindrical symmetry for each particular region. The a and c components of $\vec{v}$ are then obtained from $v_{\parallel}$ and $v_{\perp}$ by a straightforward coordinate transformation.

We turn our attention now to the $\vec{R}$ dependent factor in Eq. (2.53). Denote the direction of the applied field by the subscript i (i being either a or c in our calculations). The effective force for atomic migration; i.e., $Z_w^i eE_i$, is obtained from the $\vec{R}$ dependent force by averaging over the diffusion path. That is,

$$Z_w^i eE_i = \frac{1}{l_i} \int_{\vec{R}=\vec{R}_1}^{\vec{R}=\vec{R}_2} \vec{F}\cdot d\vec{R} \quad , \tag{2.58}$$

where $\vec{l} = \vec{R}_2 - \vec{R}_1$ is the vector which defines the diffusion jump, and

ℓ_i is its component in the i direction. This result follows simply from relating the increase (decrease) in the flow of atoms in a particular direction to the lowering (raising) of the potential barrier for diffusion. (For electromigration in the a direction in hcp Zn, Eq. (2.58) is not precisely correct. The relation is complicated by the fact that two types of crystallographically different diffusion jumps, one entirely in the basal plane, and one plane to plane (primarily in the c direction), contribute to the diffusion coefficient and to the effective charge. We will ignore this latter contribution when calculating Z_w^a. The estimated error involved in this approximation is less than 5 per cent.) Take the origin of coordinates at the point $\vec{R} = \vec{R}_1$. Using Eqs. (2.53), (2.56), and (2.57) in (2.58) gives

$$Z_w^i = -2\pi \sum_{\vec{k},\vec{k}'} \tau_i v_i(\vec{k}) \delta\left[\epsilon(\vec{k}) - \epsilon_F\right] \delta\left[\epsilon(\vec{k}) - \epsilon(\vec{k}')\right] \sum_{\vec{q}} (\vec{q})_{\ell}$$

$$\cdot \sum_{\vec{M}} \langle \phi_{\vec{k}} | e^{-i\vec{q}\cdot\vec{r}} | \phi_{\vec{k}'} \rangle \langle \phi_{\vec{k}'} | e^{i(\vec{q}+\vec{M})\cdot\vec{r}} | \phi_{\vec{k}} \rangle w^0(\vec{q}+\vec{M}) w^{0*}(\vec{q})$$

$$\cdot \frac{\int_0^{\ell} S(\vec{q},\vec{M},\vec{R})\, dR}{\ell \cos\theta_{\ell,i}} \quad , \tag{2.59}$$

where we have introduced the notation $\ell_i = \ell \cos\theta_{\ell,i}$. Of course, if the applied field is in the direction of the diffusion jump, then $(\vec{q})_{\ell} = (\vec{q})_i$ and $\cos\theta_{\ell,i} = 1$. We need only consider the real part of the integral in Eq. (2.59) since all of the other quantities are real in our model. This can be explicitly evaluated using the following result:

$$\frac{1}{\ell} \int_0^{\ell} e^{i\vec{q}\cdot\vec{R}}\, dR = \frac{e^{i\vec{q}\cdot\vec{\ell}} - 1}{i\vec{q}\cdot\vec{\ell}} \quad . \tag{2.60}$$

Eq. (2.60), together with the definition of $S(\vec{q},\vec{M},\vec{R})$ in Eq. (2.49), results in

$$\mathrm{Re}\left[\frac{1}{\ell}\int_0^{\ell} S(\vec{q},\vec{M},\vec{R})\,dR\right] \equiv \hat{S}(\vec{q},\vec{M},\vec{\ell})$$

$$= \frac{\sin(\vec{M}\cdot\vec{\ell})}{\vec{M}\cdot\vec{\ell}} - \frac{\sin(\vec{q}\cdot\vec{\ell}) - \sin(\vec{M}\cdot\vec{\ell}) + \sin[(\vec{q}+\vec{M})\cdot\vec{\ell}]}{\vec{q}\cdot\vec{\ell}} \quad . \qquad (2.61)$$

In the free electron limit, $\vec{M} = \vec{0}$ and Eq. (2.61) reduces to

$$\hat{S}(\vec{q},\vec{0},\vec{\ell}) = 1 - \frac{2\sin(\vec{q}\cdot\vec{\ell})}{\vec{q}\cdot\vec{\ell}}$$

as it should.[74]

2. Calculations and Results

For the purpose of numerical computation, the sums over $\vec{k}'$ and $\vec{k}$ in Eq. (2.59) can be transformed into integrals in the usual way; the delta functions resulting in two surface integrals over the Fermi surface. The result is

$$z_w^i = C\int_{F.S.}\int_{F.S.} \tau_i v_i(\vec{k}) \sum_{\vec{q},\vec{M}} \frac{(-\vec{q})_\ell}{\cos\theta_{\ell,i}} \langle \phi_{\vec{k}} | e^{-i\vec{q}\cdot\vec{r}} | \phi_{\vec{k}'} \rangle \langle \phi_{\vec{k}'} | e^{i(\vec{q}+\vec{M})\cdot\vec{r}} | \phi_{\vec{k}} \rangle$$

$$\cdot F(q)F(|\vec{q}+\vec{M}|)\hat{S}(\vec{q},\vec{M},\vec{\ell})\frac{dS}{v(\vec{k})}\frac{dS'}{v(\vec{k}')} \quad , \qquad (2.62)$$

where $C = \Omega_0^2/16\pi^5\hbar^2$. ($\Omega_0$ is the atomic volume.) The explicit form of the matrix elements can be seen by substituting from Eq. (2.10) for the Bloch functions $\phi_{\vec{k}}$. The result is

$$z_w^i = C\int_{F.S.}\int_{F.S.} \tau_i v_i(\vec{k}) \sum_{\vec{G},\vec{G}',\vec{K},\vec{K}'} \frac{(\vec{k}'-\vec{k}+\vec{G}'-\vec{G})}{\cos\theta_{\ell,i}} a^*_{\vec{G}}(\vec{k})a_{\vec{G}'}(\vec{K})a^*_{\vec{K}'}(\vec{k}')a_{\vec{K}}(\vec{k})$$

$$\cdot F(\vec{k}-\vec{k}'+\vec{K}-\vec{K}')F(\vec{k}'-\vec{k}+\vec{G}'-\vec{G})\hat{S}(\vec{k}'-\vec{k}+\vec{G}'-\vec{G},\vec{G}-\vec{G}'-\vec{K}+\vec{K}',\vec{\ell})\frac{dS}{v(\vec{k})}\frac{dS'}{v(\vec{k}')} \quad . \qquad (2.63)$$

Using the 2-OPW wavefunctions defined by Eqs. (2.54) and (2.55), the four-fold sum in Eq. (2.63) over reciprocal lattice vectors gives rise to 16 possible terms involving appropriate products of the functions $\alpha(\mu)$, $\beta(\mu)$, $\alpha(\mu')$, and $\beta(\mu')$. Each of the sixteen integrations must be performed separately in the full calculation.

In performing the actual integrations using our model Fermi surface, cylindrical symmetry in each region around the associated reciprocal lattice vector (Fig. B.2) allows us to write

$$\frac{dS}{v} = \frac{1}{v} k_\perp d\phi dk_\parallel \left(\frac{v}{v_\perp}\right) = \frac{m}{\hbar} d\phi dk_\parallel = \frac{mk_F}{\hbar} d\phi d\mu \quad . \tag{2.64}$$

Integration over each region is then carried out over the azimuthal angle ϕ from 0 to 2π, and over the appropriate limits of the variable μ. The integrations were done numerically using a four-dimensional trapezoidal rule. The interval sizes chosen for the numerical integration correspond to dividing the $\mu\phi$ and $\mu'\phi'$ regions each into 1728 equal area subregions. Attempts to refine the mesh further were found to be impractical in terms of computer time. The integration procedure was checked using a similar trial function and the known result was reproduced to within a per cent. Rigorous bounds on the error for the actual integrand would be difficult to estimate. We feel confident, however, that the error was no more than a few per cent, certainly insignificant considering the approximate nature of the overall calculation.

The results of the calculation are displayed in Table 2.1. The calculated values represent the electron wind contribution to the effective charge; in order to compare with the experimentally determined Z^*, the electrostatic contribution (in our model, $Z_e = +2$)

Calculation A - 1 Plane Wave, Spherical Fermi Surface

B - 1 Plane Wave, Spherical Fermi Surface (Minus missing cap areas)

C - 1 Plane Wave, Distorted Fermi Surface

D - 2 Plane Waves, Distorted Fermi Surface

	Calc. A	Calc. B	Calc. C	Calc. D	Experimental (Z^*)
Z_w^c :	-11.6	-6.4	-5.0	-4.2	-1.95 ±.15
Z_w^a :	-16.8	-9.1	-6.7	-5.7	-4.4 ±.4

Table 2.1 : Calculated Values of Z_w

must be added. The calculations were carried out in stages, each feature of the model being introduced separately to assess its quantitative effect. The first calculation was performed using a spherical Fermi surface and 1-OPW wavefunctions for the electrons. In subsequent calculations, distortion of the Fermi surface and 2-OPW wavefunctions were added. The experimental results of Routbort[39] are also displayed in Table 2.1. A complete discussion of the results is presented in PART V.

PART III

LOW-FIELD HALL EFFECT

A. Hall Effect in Anisotropic Materials

1. The Boltzmann Equation

The Boltzmann equation in the presence of both an electric field $\vec{E}$ and a magnetic field $\vec{H}$ can be written

$$\vec{v}(\vec{k}) - \frac{e}{\hbar}\left[\vec{v}(\vec{k}) \times \vec{H} \cdot \vec{\nabla}_{\vec{k}}\right]\vec{\Lambda}(\vec{k}) = \int\left[\vec{\Lambda}(\vec{k}) - \vec{\Lambda}(\vec{k}')\right] W(\vec{k},\vec{k}')\, d^3k' , \quad (3.1)$$

where $\vec{\Lambda}(\vec{k})$ is defined by

$$f(\vec{k}) - f^0(\vec{k}) = -e\left[\vec{E} \cdot \vec{\Lambda}(\vec{k})\right]\frac{\partial f^0}{\partial \epsilon} \quad . \quad (3.2)$$

We are assuming here quasi-elastic scattering between electrons on the Fermi surface; the validity of this assumption traces to the fact that the energy carried by the phonon responsible for electronic transitions in the high temperature regime is very small compared with the Fermi energy carried by the electron. $W(\vec{k},\vec{k}')$ in Eq. (3.1) represents the scattering probability when the state $\vec{k}$ is known to be occupied and $\vec{k}'$ to be unoccupied. Accordingly, W possesses the property

$$W(\vec{k},\vec{k}') = W(\vec{k}',\vec{k}) \quad . \quad (3.3)$$

Price[18] suggested expanding $f(\vec{k})$ (or equivalently, $\vec{\Lambda}(\vec{k})$) in powers of the magnetic field; i.e.,

$$\vec{\Lambda} = \vec{\lambda} + \vec{M} + \vec{N} + \ldots \quad , \quad (3.4)$$

where $\vec{\lambda}$ is independent of $\vec{H}$, $\vec{M}$ proportional to $\vec{H}$, etc. Putting Eq. (3.4) in Eq. (3.1), and equating terms with like powers of $\vec{H}$ gives

$$\vec{v} = \int(\vec{\lambda} - \vec{\lambda}')\, W\, d^3k' \quad , \quad (3.5a)$$

$$-\frac{e}{\hbar}\left[\vec{v} \times \vec{H} \cdot \vec{\nabla}\right] \vec{\lambda} = \int (\vec{M} - \vec{M}') \, W \, d^3k' \quad , \tag{3.5b}$$

$$-\frac{e}{\hbar}\left[\vec{v} \times \vec{H} \cdot \vec{\nabla}\right] \vec{M} = \int (\vec{N} - \vec{N}') \, W \, d^3k' \quad , \tag{3.5c}$$

etc.

In calculating the Hall effect to terms linear in the magnetic field, only Eqs. (3.5a) and (3.5b) need be considered. It appears then that calculating the linear Hall effect involves solving two successive integral equations; i.e., first solving Eq. (3.5a) for $\vec{\lambda}$ as in the conductivity analysis of Chan and Huntington,[22] then substituting this result in Eq. (3.5b) and solving for $\vec{M}$. However, Price has shown that in reality only Eq. (3.5a) need be solved (for the linear Hall effect). The reason for this is that we really do not need to explicitly evaluate the vector function $\vec{M}$. We only need to calculate its effect on the current density $\vec{J}$; i.e., we need to calculate

$$\vec{J} = -\frac{e^2}{4\pi^3} \vec{E} \cdot \int \vec{\lambda}(\vec{k}) \, \vec{v}(\vec{k}) \, \frac{\partial f^0}{\partial \epsilon} \, d^3k$$

$$\simeq -\frac{e^2}{4\pi^3} \vec{E} \cdot \left[\int \vec{\lambda} \, \vec{v} \, \frac{\partial f^0}{\partial \epsilon} \, d^3k + \int \vec{M} \, \vec{v} \, \frac{\partial f^0}{\partial \epsilon} \, d^3k \, . \right] \tag{3.6}$$

As before, we assume the solution of Eq. (3.5a) is known from previous work. This allows us to calculate the first of the integrals in Eq. (3.6). Starting with Eq. (3.5b), we arrive at an expression for the second integral as follows. Multiplying both sides of Eq. (3.5b) by $\vec{\lambda} \frac{\partial f^0}{\partial \epsilon}$, integrating over $\vec{k}$, and rearranging on the left yields

$$\frac{e}{\hbar} \vec{H} \cdot \int (\vec{v} \times \vec{\nabla} \vec{\lambda}) \, \vec{\lambda} \, \frac{\partial f^0}{\partial \epsilon} \, d^3k = \iint \vec{M} \, \vec{\lambda} \, \frac{\partial f^0}{\partial \epsilon} \, W(\vec{k},\vec{k}') \, d^3k \, d^3k'$$

$$- \iint \vec{M}' \vec{\lambda} \, \frac{\partial f^0}{\partial \epsilon} \, W(\vec{k},\vec{k}') \, d^3k \, d^3k' \quad . \tag{3.7}$$

Interchanging $\vec{k}$ and $\vec{k}'$ in the second integral, and using Eq. (3.3), we get

$$\frac{e}{\hbar}\vec{H}\cdot\int(\vec{v}\times\vec{\nabla}\vec{\lambda})\,\vec{\lambda}\,\frac{\partial f^0}{\partial\epsilon}\,d^3k = \int\vec{M}\left[\int(\vec{\lambda}\,\frac{\partial f^0}{\partial\epsilon} - \vec{\lambda}'\frac{\partial f^0}{\partial\epsilon'})\,W\,d^3k'\right]d^3k$$

$$= \int\vec{M}\,\vec{v}\,\frac{\partial f^0}{\partial\epsilon}\,d^3k \quad . \tag{3.8}$$

(The elastic scattering assumption allowed us to replace $\frac{\partial f^0}{\partial\epsilon'}$ by $\frac{\partial f^0}{\partial\epsilon}$.) The right hand side of Eq. (3.8) is seen to be the integral required in Eq. (3.6). Thus the current for the linear Hall effect is given by $\frac{e}{\hbar}\vec{H}\cdot\int(\vec{v}\times\vec{\nabla}\vec{\lambda})\,\vec{\lambda}\,\frac{\partial f^0}{\partial\epsilon}\,d^3k$, and depends only on the properties of $\vec{\lambda}$ calculated from Eq. (3.5a).

2. The Onsager Reciprocal Relations

In this section we write down some general results deriving from the Onsager relations. They will be used in a later section in applying our model of the Fermi surface. The Onsager relation[77] for electrical conduction in the presence of a magnetic field states that

$$\overline{\overline{\sigma}}\,(\vec{H})^{\sim} = \overline{\overline{\sigma}}\,(-\vec{H}) \quad , \tag{3.9}$$

where $\overline{\overline{\sigma}}$ is the conductivity tensor and $\sim$ denotes the transpose. In order that our calculated results possess the required reciprocity, Eqs. (3.5) and (3.9) require that $\int\vec{\lambda}\,\vec{v}\,\frac{\partial f^0}{\partial\epsilon}\,d^3k$ be a symmetric tensor, and that $\int\vec{M}\,\vec{v}\,\frac{\partial f^0}{\partial\epsilon}\,d^3k$ be antisymmetric. The first condition follows immediately from Eqs. (3.5a) and (3.3). Using Eq. (3.8), we see that the second condition requires that $\vec{H}\cdot\int(\vec{v}\times\vec{\nabla}\vec{\lambda})\,\vec{\lambda}\,\frac{\partial f^0}{\partial\epsilon}\,d^3k$ be antisymmetric, or equivalently that $\vec{H}\cdot\int_{F.S.}(d\vec{S}\times\vec{\nabla}\vec{\lambda})\,\vec{\lambda}$ be antisymmetric. (Here $d\vec{S}$ is the vector element of surface area on the Fermi surface.) To see what is going on here, we write $\vec{\nabla}\vec{\lambda}$ as a sum of dyads:

$$\vec{\nabla}\vec{\lambda} = \sum_i \vec{a}_i \vec{b}_i \quad . \tag{3.10}$$

Using Eq. (3.10), the antisymmetry condition becomes

$$\int_{F.S.} \vec{H} \cdot (d\vec{S} \times \sum \vec{a}_i \vec{b}_i \vec{\lambda}) = -\int_{F.S.} \vec{H} \cdot (d\vec{S} \times \sum \vec{a}_i \vec{\lambda} \vec{b}_i)$$

or

$$\vec{H} \cdot \int_{F.S.} d\vec{S} \times \left\{ (\vec{\nabla}\vec{\lambda})\vec{\lambda} + \sum_i \vec{a}_i \vec{\lambda} \vec{b}_i \right\} = 0 \quad . \tag{3.11}$$

The quantity in $\{\}$ is just $\vec{\nabla}(\vec{\lambda}\vec{\lambda})$; thus, the reciprocity condition will be satisfied if

$$\int_{F.S.} d\vec{S} \times \vec{\nabla}(\vec{\lambda}\vec{\lambda}) = 0 \quad . \tag{3.12}$$

If the Fermi surface is a smooth, continuous closed surface, Eq. (3.12) is shown to be true by dividing the surface in two parts, and applying the generalized Stokes Theorem to each part. The two line integrals which result cancel exactly. For a surface cut by Brillouin zone walls, Stokes Theorem gives

$$\int d\vec{S} \times \vec{\nabla}(\vec{\lambda}\vec{\lambda}) = \sum_C \oint_C d\vec{k}\, (\vec{\lambda}\vec{\lambda}) \quad , \tag{3.13}$$

where each term in the sum is a line integral over the boundary curve of an open portion of the Fermi surface. The sum in Eq. (3.13) is seen to be zero by considering contributions from curves on opposite faces of the Brillouin zone; since they are displaced by a reciprocal lattice vector, symmetry requires $\vec{\lambda}$ to be the same for corresponding points, whereas the direction of integration is opposite (as dictated by proper application of Stokes Theorem). Thus our solutions will have the required Onsager symmetry, provided we use a continuous, smooth Fermi surface, interrupted only by Brillouin zone discontinuities. Our

model surface (APPENDIX B) does not meet that requirement, however. This point will be discussed in section III.B.3.

3. Expressions for the Hall Coefficients

The Hall constant as customarily defined is given by the ratio of the transverse electric field to the product of the current density (in the direction of the applied electric field) and the magnetic field. For example, if the experimental geometry is such that the current is constrained to flow in the "y" direction, and the magnetic field applied in the "z" direction, then the Hall coefficient is given by $R = \frac{-E_x}{J_y H_z}$. (x,y, and z form a right-handed coordinate system and the sign of R is such that free electron conduction produces a negative Hall coefficient.) The Onsager relations allow at most three independent Hall coefficients, depending only on the direction of the applied magnetic field. For $\vec{H}$ in the x direction, one obtains using Eqs. (3.6) and (3.9)

$$R(H_x) = \frac{E_z}{J_y H_x}\bigg|_{J_z=0} = -\frac{C}{H_x \sigma_{yy} \sigma_{zz}} \int M_y v_z \frac{dS}{v} \tag{3.14a}$$

$$- = \frac{-E_y}{J_z H_x}\bigg|_{J_y=0} = \frac{C}{H_x \sigma_{yy} \sigma_{zz}} \int M_z v_y \frac{dS}{v} \tag{3.14b}$$

Similarly,

$$R(H_y) = \frac{E_x}{J_z H_y}\bigg|_{J_x=0} = -\frac{C}{H_y \sigma_{xx} \sigma_{zz}} \int M_z v_x \frac{dS}{v} \tag{3.15a}$$

$$= \frac{-E_z}{J_x H_y}\bigg|_{J_z=0} = \frac{C}{H_y \sigma_{xx} \sigma_{zz}} \int M_x v_z \frac{dS}{v} \tag{3.15b}$$

$$R(H_z) = \frac{E_y}{J_x H_z}\bigg|_{J_y=0} = -\frac{C}{H_z \sigma_{xx} \sigma_{yy}} \int M_x v_y \frac{dS}{v} \tag{3.16a}$$

$$= \frac{-E_x}{J_y H_z}\bigg|_{J_x=0} = \frac{C}{H_z \sigma_{xx} \sigma_{yy}} \int M_y v_x \frac{dS}{v} \qquad (3.16b)$$

where $C = 4\pi^3\hbar/e^2$ and $\sigma_{ii} = \int \lambda_i v_i \frac{dS}{v}$ is proportional to the conductivity in the absence of a magnetic field. (All of the integrations in Eqs. (3.14)-(3.16) are over the Fermi surface.) The expressions in the numerators of Eqs. (3.14)-(3.16) can be evaluated in terms of the vector function $\vec{\lambda}$ and its derivatives by making use of Eq. (3.8). Making the appropriate substitutions, we arrive at our final expressions for the three independent Hall constants:

$$R(H_i) = \frac{4\pi^3}{e \sigma_{jj} \sigma_{kk}} \int (v_j \frac{\partial \lambda_k}{\partial k_k} - v_k \frac{\partial \lambda_k}{\partial k_j}) \lambda_j \frac{dS}{v} \qquad (3.17)$$

where e is taken to be the (negative) electronic charge, and i,j,k represent a permutation of the variables x,y, and z. (The two expressions for $R(H_i)$ generated by interchanging j and k in Eq. (3.17) are of course equal as a result of the Onsager relation.)

B. Application to Zinc

1. General Formulas

As before, we take $\lambda_k = \tau_k v_k$ and substitute into Eq. (3.17) to get

$$R(H_i) = \frac{4\pi^3}{e \int \tau_j v_j^2 \frac{dS}{v} \cdot \int \tau_k v_k^2 \frac{dS}{v}} \left[\int \tau_k \tau_j (v_j \frac{\partial v_k}{\partial k_k} - v_k \frac{\partial v_k}{\partial k_j}) v_j \frac{dS}{v} + \int v_j v_k (v_j \frac{\partial \tau_k}{\partial k_k} - v_k \frac{\partial \tau_k}{\partial k_j}) \tau_j \frac{dS}{v} \right] . \qquad (3.18)$$

The second integral in Eq. (3.18) contains $(\vec{v} \times \vec{\nabla}\tau)_i$, and thus involves

non-uniformities in τ from point to point on the Fermi surface (since $\vec{v}$ is perpendicular to the surface). For $R(H_z)$, only the directional derivatives of τ along orbits parallel to the basal plane enter. However, the Chan, Huntington calculations[22,81] demonstrated that this variation is slight in general, justifying its neglect here. For $R(H_x)$ (or $R(H_y)$) the situation is not quite so clear. In these cases the variation of τ with μ, as shown in Fig. C.2, is involved. The deviations of τ from $\langle\tau\rangle$ still appear small, though not so clearly negligible as in the first case. From a practical point of view, it is doubtful whether the calculated data are accurate enough to justify inferring values of the derivatives of τ on a point by point basis. Nevertheless, using the data of Fig. C.2 and a spherical Fermi surface corrected for the missing area (see Fig. 4.2), a rough estimate of the second integral in Eq. (3.18) was calculated. The calculation proved to be a fairly sensitive one, owing to close cancellation between regions of positive and negative $\frac{\partial\tau}{\partial\mu}$. The calculated estimate was roughly 20 per cent of the contribution from the first integral, and of the same sign.[-] In what follows, the contributions from $\vec{\nabla}\tau$ are not included.

For Zn, hexagonal symmetry reduces the number of independent Hall constants to two, one with the magnetic field in the c direction, and the other with the magnetic field in the basal plane. Choosing our z-axis along the hexad symmetry axis, we need to consider $R(H_z)$ and either $R(H_x)$ or $R(H_y)$. We make the following definitions: $R_{\parallel} = R(H_z)$ and $R_{\perp} = R(H_y)$. From Eq. (3.18), we arrive at the following expressions (with $\lambda_i = \langle\tau_i\rangle v_i$) :

$$R_{\parallel} = \frac{4\pi^3}{e} \frac{\int (v_y \frac{\partial v_x}{\partial k_x} - v_x \frac{\partial v_x}{\partial k_y}) v_y \frac{dS}{v}}{\int v_x^2 \frac{dS}{v} \cdot \int v_y^2 \frac{dS}{v}} \tag{3.19a}$$

$$= (x \leftrightarrow y) \tag{3.19b}$$

$$R_{\perp} = \frac{4\pi^3}{e} \frac{\int (v_x \frac{\partial v_z}{\partial k_z} - v_z \frac{\partial v_z}{\partial k_x}) v_x \frac{dS}{v}}{\int v_x^2 \frac{dS}{v} \cdot \int v_z^2 \frac{dS}{v}} \tag{3.20a}$$

$$= (x \leftrightarrow z) \tag{3.20b}$$

where the notation $(x \leftrightarrow y)$ means interchange the variables x and y in the preceding expression. Eqs. (3.19) and (3.20) are the starting points for our numerical computations.

In performing the required calculations for our Fermi surface model, we encounter a difficulty suggested in section III.A.2. The Onsager relations require that our model yield the same results whether the a or b versions of the above equations are used. By symmetry considerations alone, it is easily seen that Eqs. (3.19a) and (3.19b) will give the same result. However, expressions (3.20a) and (3.20b) do not, in general, give the same result. The problem arises because we have introduced artificial boundaries in our model surface; the free surface area is divided up into cylindrically symmetric regions about the appropriate reciprocal lattice vectors. There is a certain amount of arbitrariness in the relative size of these regions. We can, at least in our model for Zn, remove this arbitrariness by selecting our boundaries so that the Onsager relations are satisfied. The required condition from Eq. (3.13) is, in general,

$$\sum_C \oint_C d\vec{k} \, (\hat{\lambda}\hat{\lambda}) = 0 \quad . \tag{3.21}$$

The particular component of the triad of interest here is the $\hat{j}\,\hat{i}\,\hat{k}$ component; the condition we need to satisfy in order that Eqs. (3.20a) and (3.20b) give the same result is

$$\sum_C \oint_C dk_y v_x v_z = 0 \quad . \tag{3.22}$$

The sum over the curves C representing intersections with Brillouin zones gives zero (as was previously argued), which leaves the line integrals over the artificial boundaries introduced. The limits of integration in each region were varied (actually, symmetry and the requirement of constancy of free Fermi surface area reduced the number of variable parameters to one) until the sum in Eq. (3.22) was forced to zero. This determined the limits of integration used in the final calculations.

2. Calculations at High Temperature (650 K)

In calculating the Hall constants the following procedure was used. In each cylindrically symmetric region, the tensor $\vec{H} \cdot \int (\vec{v} \times \vec{\nabla}\vec{v})\vec{v} \frac{dS}{v}$ was calculated with the z-axis chosen along the axis of symmetry. This made $\vec{\nabla}\vec{v}$ diagonal and also simplified the expressions for $\vec{v}$. These are given explicitly in APPENDIX B. Then a straightforward similarity transformation was used to transform the result to a coordinate system with z-axis in the c direction. The calculated tensor $\vec{H} \cdot \int (\vec{v} \times \vec{\nabla}\vec{v})\vec{v} \frac{dS}{v}$ proved to be antisymmetric, which verified the procedure described in the previous section for selecting the limits of integration. The integrals in the denominators

of Eqs. (3.19) and (3.20) were calculated in a similar manner.

The high temperature Fermi surface parameters relevant to our model are shown in Table B.1. The calculated results, in units of m^3/coul., are

$$R_{\parallel} = +8.2 \times 10^{-11}$$

$$R_{\perp} = -1.3 \times 10^{-11} \quad .$$

By comparison, the free electron value for Zn is about -4.75×10^{-11}. The values are shown in Fig. 3.1, along with several experimentally determined values.

3. Temperature Dependence

Of course, a complete temperature analysis would require resolving the Boltzmann equation for $\vec{\lambda}(\vec{k})$ at another temperature or set of temperatures. Short of this, if we choose another temperature and again make the approximation that $\lambda_i = \langle \tau_i \rangle v_i$ at this new temperature, τ again disappears from our expressions for $R_{\parallel}$ and $R_{\perp}$. These expressions depend only on the size and shape of the Fermi surface whose temperature dependence can be handled approximately within our model. 400 K was chosen as the temperature for a second set of calculations, and the relevant lattice and Fermi surface parameters were recalculated. A comparison between these values and those given in APPENDIX B for 650 K is given in Table 3.1. The values of c and a were recalculated using the thermal expansion data of Gilder and Wallmark.[80] In addition to changing the c/a ratio, increasing the temperature tends to decrease the Debye-Waller factors[85] (e^{-2W}) and thus decreases the band gaps responsible for Fermi surface distortion. The results of the calculations at 400 K are also shown in Fig. 3.1.

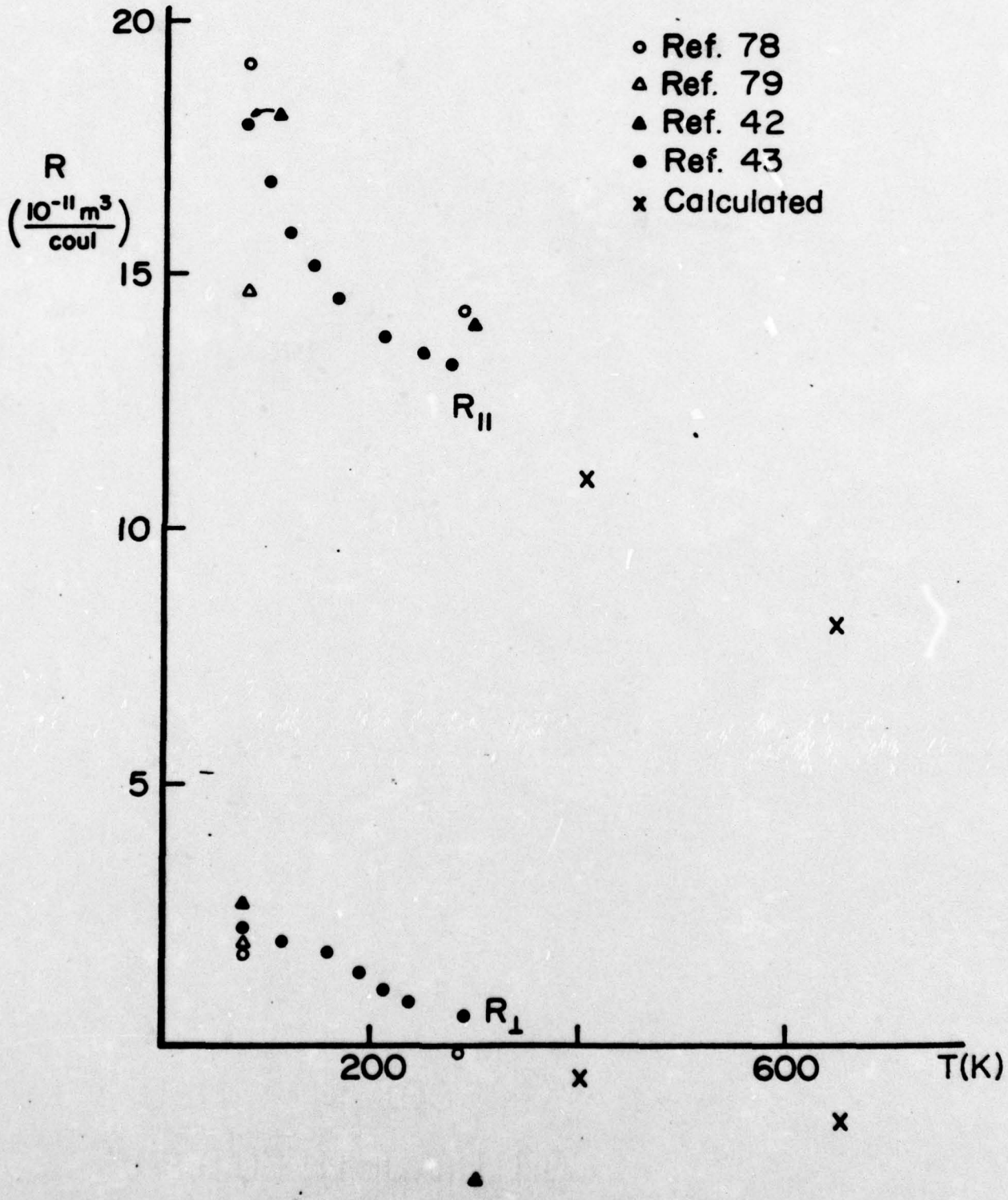

Fig. 3.1: Hall Constants vs. Temp.

	c (A°)	a (A°)	γ_{101}	$e^{-2W_{101}}$	g_{101}	γ_{002}	$e^{-2W_{002}}$	g_{002}
400 K :	4.98	2.66	.955	.864	.050	.803	.795	.026
650 K :	5.05	2.67	.957	.758	.047	.798	.649	.023

Table 3.1 : Lattice and Fermi Surface Parameters

The available experimental data for the Hall effect in Zn single crystals extend only to about 300 K. However, polycrystalline data[54,86] for both Zn and Cd decrease approximately linearly with temperature in the region beyond 300 K. In addition, single crystal measurements for both $R_{\parallel}$ and $R_{\perp}$ in Cd[87] show a roughly linear decrease with temperature in this range; all of which suggests a linear extrapolation of the experimental data in Fig. 3.1 for Zn. Our calculated values, also shown in Fig. 3.1, would apparently agree quite well with any reasonable extrapolation.

PART IV

THERMOELECTRIC POWER

A. General Theory

In the presence of a temperature gradient, the Boltzmann equation for the conduction electrons becomes (again assuming quasi-elastic scattering)

$$\left(-\frac{\partial f^0}{\partial \epsilon}\right) \vec{v} \cdot \left[e\vec{E} - (\epsilon - \epsilon_F)\frac{\vec{\nabla} T}{T} \right] = \int \left[g(\vec{k}) - g(\vec{k}') \right] W(\vec{k},\vec{k}') \, d^3k' \quad . \tag{4.1}$$

Extending the mean free path formalism, one may define $\vec{\lambda}$ by

$$g(\vec{k}) = \left(-\frac{\partial f^0}{\partial \epsilon}\right) \left[e\vec{E} - (\epsilon - \epsilon_F)\frac{\vec{\nabla} T}{T} \right] \cdot \vec{\lambda} \quad . \tag{4.2}$$

Substitution of Eq. (4.2) in (4.1) results in the simpler form of the Boltzmann equation,

$$\vec{v}(\vec{k}) = \int \left[\vec{\lambda}(\vec{k}) - \vec{\lambda}(\vec{k}') \right] W(\vec{k},\vec{k}') \, d^3k' \quad . \tag{4.3}$$

In anisotropic materials, the absolute thermoelectric power (TEP) is defined by

$$E_i = S_i (\vec{\nabla} T)_i \quad , \tag{4.4}$$

where the subscript i denotes the direction of the temperature gradient. In terms of $\vec{\lambda}$, the resulting expression for S_i becomes

$$S_i = \frac{\pi^2 k_B^2 T}{3e} \left[\frac{1}{\sigma_i(\epsilon)} \frac{\partial \sigma_i}{\partial \epsilon} \right]_{\epsilon = \epsilon_F} \quad , \tag{4.5}$$

where $\sigma_i(\epsilon)$ is given by

$$\sigma_i(\epsilon) = \frac{e^2}{4\pi^3} \int \lambda_i v_i \frac{dS}{|\vec{v}|} \quad . \tag{4.6}$$

In Eq. (4.6), the integration is over a surface of constant energy ϵ. Eq. (4.5) is to be interpreted as follows. It means that one should calculate the conductivity as a function of the hypothetical height, ϵ, of the Fermi level, and then evaluate the derivative of $\sigma(\epsilon)$ with respect to ϵ at the actual Fermi energy, ϵ_F. The variation of σ with energy will depend on the change in the numbers of electrons available for conduction, as well as the change of the mean free path of each electron as its energy changes.

With $\lambda_i = \tau_i v_i$, Eq. (4.6) becomes

$$\sigma_i = \frac{e^2}{4\pi^3}\int \tau_i v_i^2 \frac{dS}{v} \equiv \frac{e^2}{4\pi^3}\langle\tau_i\rangle\int v_i^2 \frac{dS}{v} \equiv \frac{e^2}{4\pi^3}\langle\tau_i\rangle X_i \quad , \qquad (4.7)$$

where $X_i = \int v_i^2 \frac{dS}{v}$, and $\langle\rangle$ denotes the appropriate average value. Substituting Eq. (4.7) in (4.5) gives

$$S_i = \frac{\pi^2 k_B^2 T}{3e\epsilon_F}\left[\frac{\epsilon_F}{X_i}\frac{\partial X_i}{\partial \epsilon} + \frac{\epsilon_F}{\langle\tau_i\rangle}\frac{\partial\langle\tau_i\rangle}{\partial\epsilon}\right]_{\epsilon=\epsilon_F} . \qquad (4.8)$$

Eq. (4.8) is the form in which the TEP is often analyzed. Since e is negative, the factor preceding the dimensionless quantities in brackets is negative and typically of the order of one microvolt per degree K. The first term in the brackets in Eq. (4.8), call it s_{1i}, involves only the geometry of the Fermi surface, and has the value 3/2 in the FEM. Ignoring the second term for the moment, this would predict a negative TEP. In his analysis of the noble metals, Ziman[41] showed that the effect of Fermi surface anisotropy was to reduce s_1, but not enough to drive it negative and account for the positive values of TEP observed experimentally. The experimental results were only

understood after a careful analysis of the term involving $\langle\tau\rangle$, which we shall hereafter call s_2.

B. Application to Zinc

1. Fermi Surface Model

In our TEP calculations for Zn, we chose a simplified model Fermi surface illustrated in Fig. 4.1. The surface is spherical, and 1-OPW electron wavefunctions are used throughout. The missing area (APPENDIX B) was accounted for approximately by multiplying each element of surface area by $P(\mu)$, where $P(\mu)$ is given by

$$P(\mu) = \begin{cases} 1, & |\mu| > \mu_{max} \\ 1 - \frac{6}{\pi}\phi_m, & \mu_{max} > |\mu| > \mu_{min} \\ 1, & |\mu| < \mu_{min} \end{cases} \qquad (4.9)$$

and

$$\cos\phi_m = \frac{\gamma_{101} - \mu\cos\theta_{101}}{\rho\sin\theta_{101}} \quad , \qquad (4.10)$$

θ_{101} being the angle between the reciprocal lattice vectors $\vec{Q}_3$ (see Eqs. (4.15)) and the c-axis. In equations (4.9) and (4.10), the quantities μ_{max}, μ_{min}, and γ_{101} will of course depend on ϵ, the hypothetical Fermi level in Eq. (4.8). This approximate treatment of the missing area assumes it to be uniformly distributed in the ϕ direction.

2. Solution of the Boltzmann Equation

Following Chan and Huntington,[22] we write $\lambda_i = \tau_i v_i$, from which it follows that

$$\tau_i(\vec{k}) \simeq \frac{v_i(\vec{k})}{\int\left[v_i(\vec{k}) - v_i(\vec{k}')\right] W(\vec{k},\vec{k}')\, d^3k'} \equiv \frac{v_i(\vec{k})}{I(\vec{k})} \quad . \qquad (4.11)$$

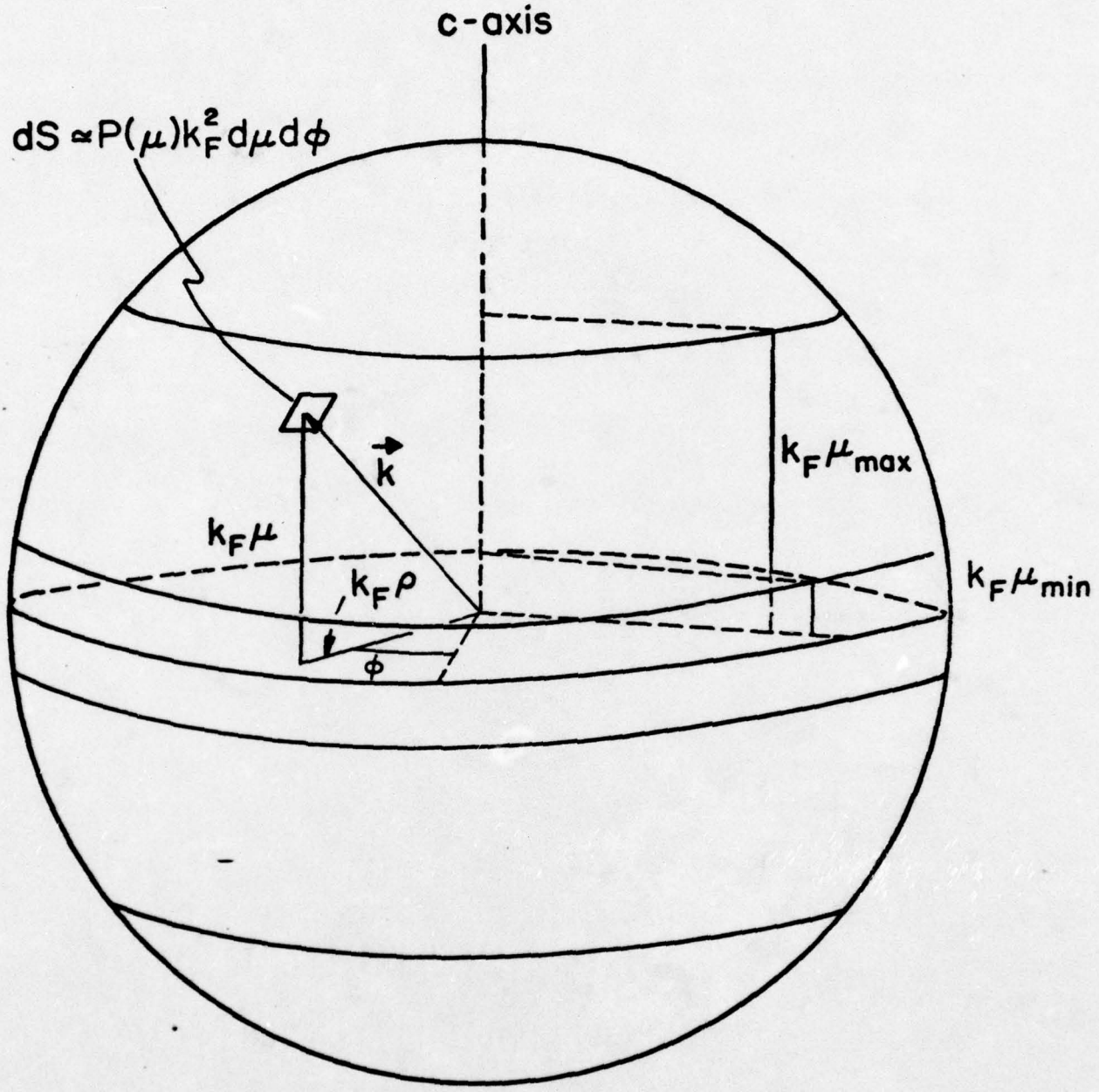

Fig. 4.1: Fermi Surface Model (TEP Calculation)

Strictly speaking, Eq. (4.11) actually represents the first term in an iterative expansion for τ_i. However, subsequent terms were shown to be very small, and we shall therefore use Eq. (4.11) for τ_i in this calculation. What is needed then is a solution for τ_a and τ_c as a function of the hypothetical Fermi level, ϵ. In the actual calculation, the energy derivatives were estimated by calculating $\tau_i(\epsilon=\epsilon_F)$ and $\tau_i(\epsilon=\epsilon_F + \Delta\epsilon_F)$, with Δ taken to be .002.

We next describe an explicit form for the scattering kernel $W(\vec{k},\vec{k}')$, the basic transition probability from state $\vec{k}$ to $\vec{k}'$. We use the "rigid ion" model[82] for the electron phonon interaction, along with a local pseudopotential approximation. The optical phonon branches are accounted for by using the double (or Jones) zone (Fig. B.1) for the phonon cells. Although this has a complex shape, it is not too far from spherical; we therefore replace the actual phonon cells by Debye spheres. The experimental phonon dispersion curves and our analytic fits to these curves are described in APPENDIX C and illustrated in Figs. C.1 and C.2 respectively.

The contribution of normal phonon processes (I_N) to the integral $I(\vec{k})$ is given by

$$I_N(\vec{k}) = C \int dS' (-\vec{q})_i \frac{q^2}{\omega_{qL}^2} F^2(q) \quad , \tag{4.12}$$

where $\vec{q} = \vec{k}' - \vec{k}$ is the phonon wave vector, $F(q)$ the pseudopotential form factor, ω_{qL} the (longitudinal) phonon frequency, and

$$C = \frac{k_B T}{4\pi^2 \hbar^2 k_F nNM} \quad . \tag{4.13}$$

In Eq. (4.13), k_F is the Fermi wavevector, n the number of ions per unit cell (2 for Zn), N the number of cells per unit volume, and M is the ionic mass. The domain of integration over $\vec{k}'$ implicit in Eq. (4.12) is determined by the intersection of the Debye and Fermi spheres, and is illustrated in Fig. 4.2(a). The contribution of umklapp processes is given by

$$I_U(\vec{k}) = C \int dS' \left[-(\vec{q} + \vec{Q})\right]_i J^2(\vec{q},\vec{Q})\, F^2(\vec{q}+\vec{Q})\, S^2_{\vec{Q}} \quad , \qquad (4.14)$$

where $\vec{q} + \vec{Q} = \vec{k}' - \vec{k}$ and $\vec{Q}$ is a reciprocal lattice vector. $S_{\vec{Q}}$ is the structure factor for $\vec{Q}$ defined in the usual way by

$$S_Q = \left| \frac{1}{n} \sum_{m=0}^{n-1} e^{i\vec{Q}\cdot\vec{r}_m} \right| \quad , \qquad (4.15)$$

where $\vec{r}_m$ specifies the position of each atom within the unit cell. $J^2(\vec{q},\vec{Q})$ is defined by

$$J^2(\vec{q},\vec{Q}) = \frac{\left[\vec{e}_q \cdot (\vec{q} + \vec{Q})\right]^2}{\omega^2_{qL}} + \frac{(|\vec{e}_q \times \vec{Q}|)^2}{\omega^2_{qT}} \quad , \qquad (4.16)$$

$\vec{e}_q$ being a unit vector in the $\vec{q}$ direction, and ω_{qT} means the polarization is transverse and lying in the $\vec{q}$-$\vec{Q}$ plane. The geometry for umklapp scattering and the domain of integration for Eq. (4.14) are schematically illustrated in Fig. 4.2(b).

3. Calculations

In computing the umklapp integrals, contributions from four types of RLV's were considered. With the z direction along the crystal c-axis, the components of the RLV's considered are

$$\vec{Q}_1 : \frac{4\pi}{c}(0,0,\pm 1) \quad ,$$

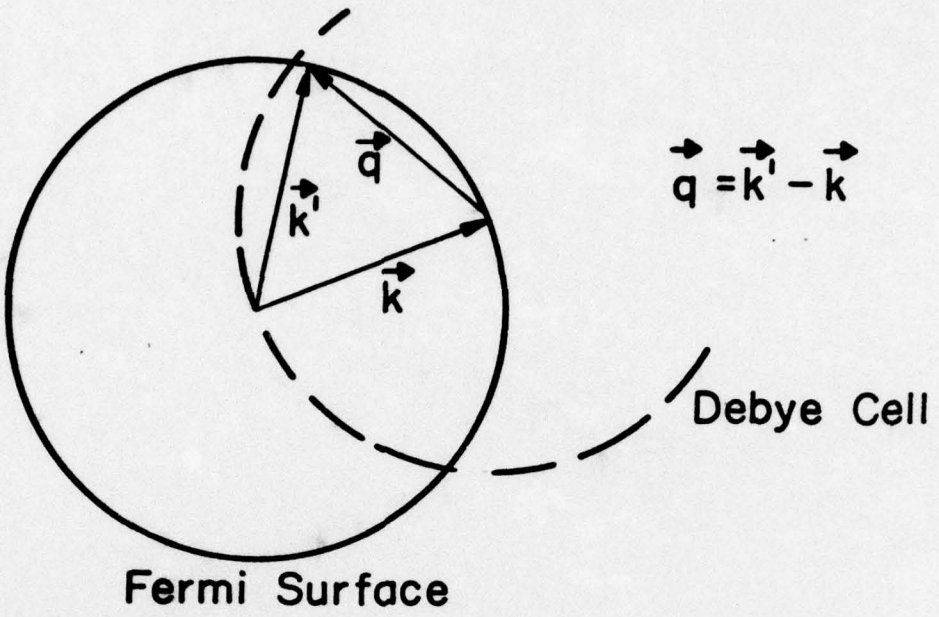

(a) Normal

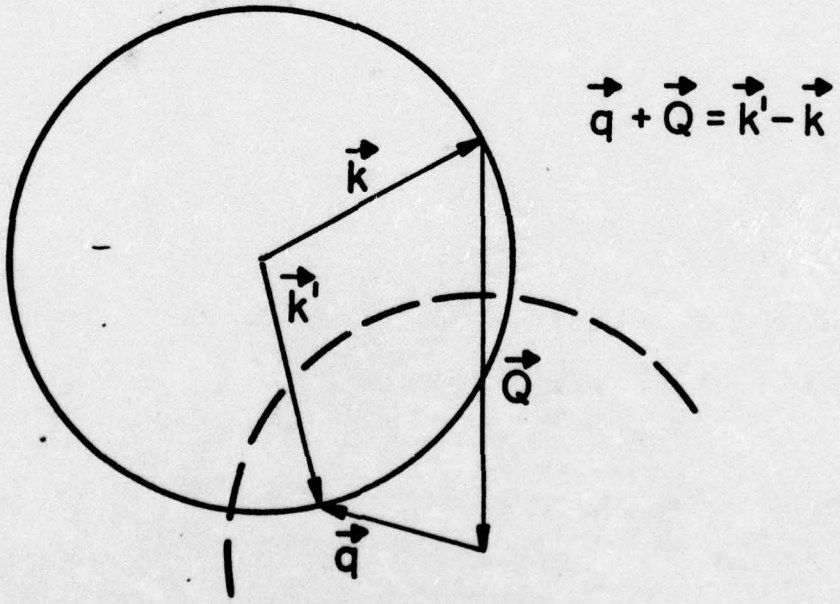

(b) Umklapp

Fig. 4.2: Geometry for Normal and Umklapp Scattering

$$\vec{Q}_2 : \frac{4\pi}{\sqrt{3}\,a}\left(\pm\frac{\sqrt{3}}{2}, \pm\frac{1}{2}, 0\right) \quad , \quad \frac{4\pi}{\sqrt{3}\,a}(0, \pm 1, 0) \quad ,$$
$$\vec{Q}_3 = \vec{Q}_2 + \tfrac{1}{2}\vec{Q}_1 \quad , \tag{4.17}$$
$$\vec{Q}_4 = \vec{Q}_2 + \vec{Q}_1 \quad .$$

Of these 32 RLV's, 18 give non-zero contributions. The surface integrations were performed numerically, and the area elements used were roughly 1/8,000 of the total Fermi sphere area.

The first set of calculations was performed using the model form factor described in APPENDIX A (dotted line in Fig. A.1). The calculated values of τ_a and τ_c are plotted vs. μ in Fig. 4.3. (We should point out that a singularity in the scattering kernel occurs near $\mu = .8$, as $\vec{k}$ reaches the Brillouin zone. This type of singularity is known to be a result of the FEM; it does not occur when the proper Bloch wavefunctions are used. The plotted results represent a smooth continuation over the singularity.) The comparable results from Ref. 22 are shown in Fig. C.3. Results of the TEP calculations for S_a and S_c are given in Table 4.1, along with values of the dimensionless quantities $\bar{s}_1$ and s_2. Results of a second set of calculations using the semi-empirical form factor (APPENDIX A) are also given in Table 4.1. Fig. 4.4 displays the theoretical values and the experimental results of Rowe and Schroeder.[55]

The experimental data for Zn single crystals are quite sparse, extending only to about room temperature. As in the Hall effect, a straight line extrapolation to high temperature is again suggested by the available polycrystalline data.[54] Based on this assumption, our

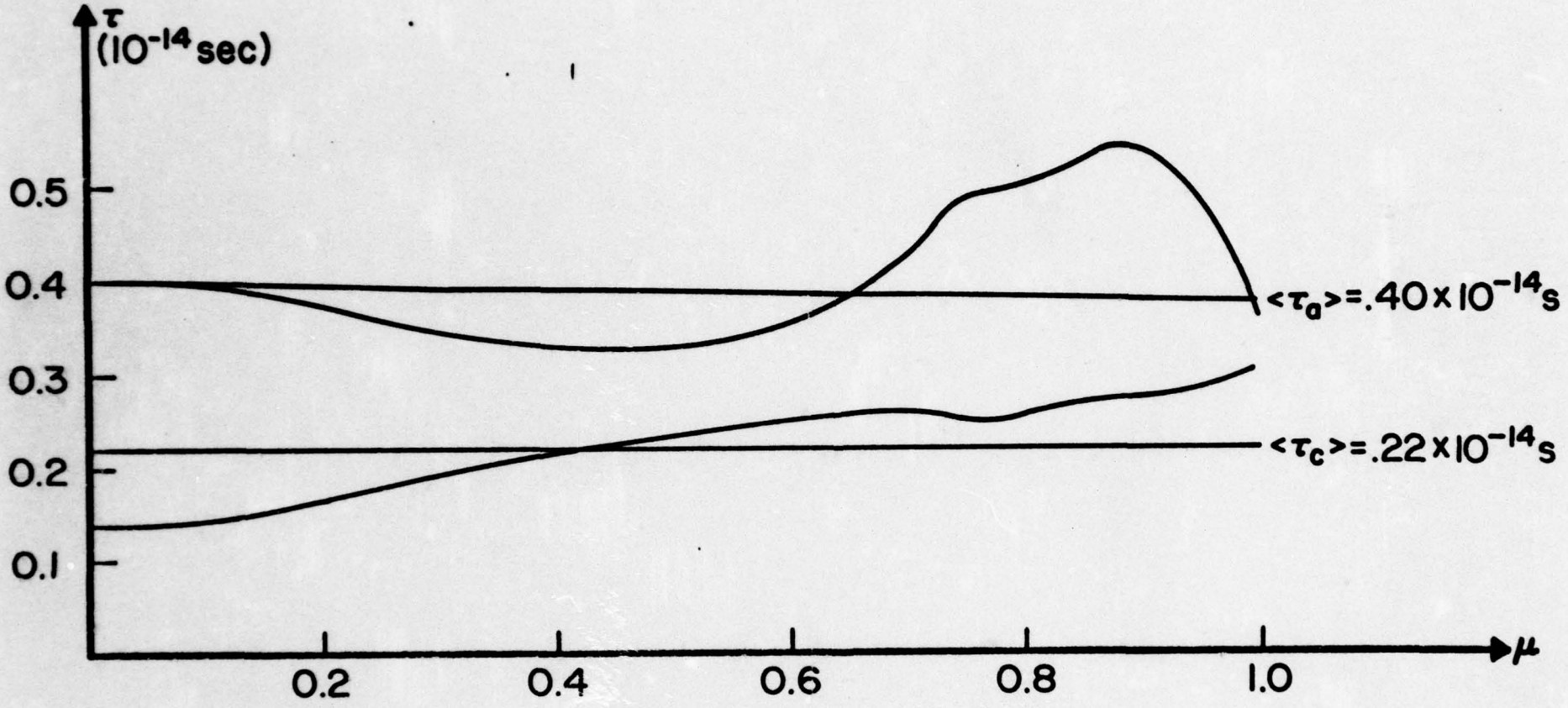

Fig. 4.3: Calculated Values of τ vs. μ

	s_{1a}	s_{2a}	S_a $(\frac{\mu V}{K})$	s_{1c}	s_{2c}	S_c $(\frac{\mu V}{K})$
Model Form Factor :	-4.03	-.56	+7.87	-.71	-.27	+1.69
Semi-empirical Form Factor :	-4.03	-2.38	+10.87	-.71	-2.22	+5.02

Table 4.1 : Results of Thermoelectric Power Calculations

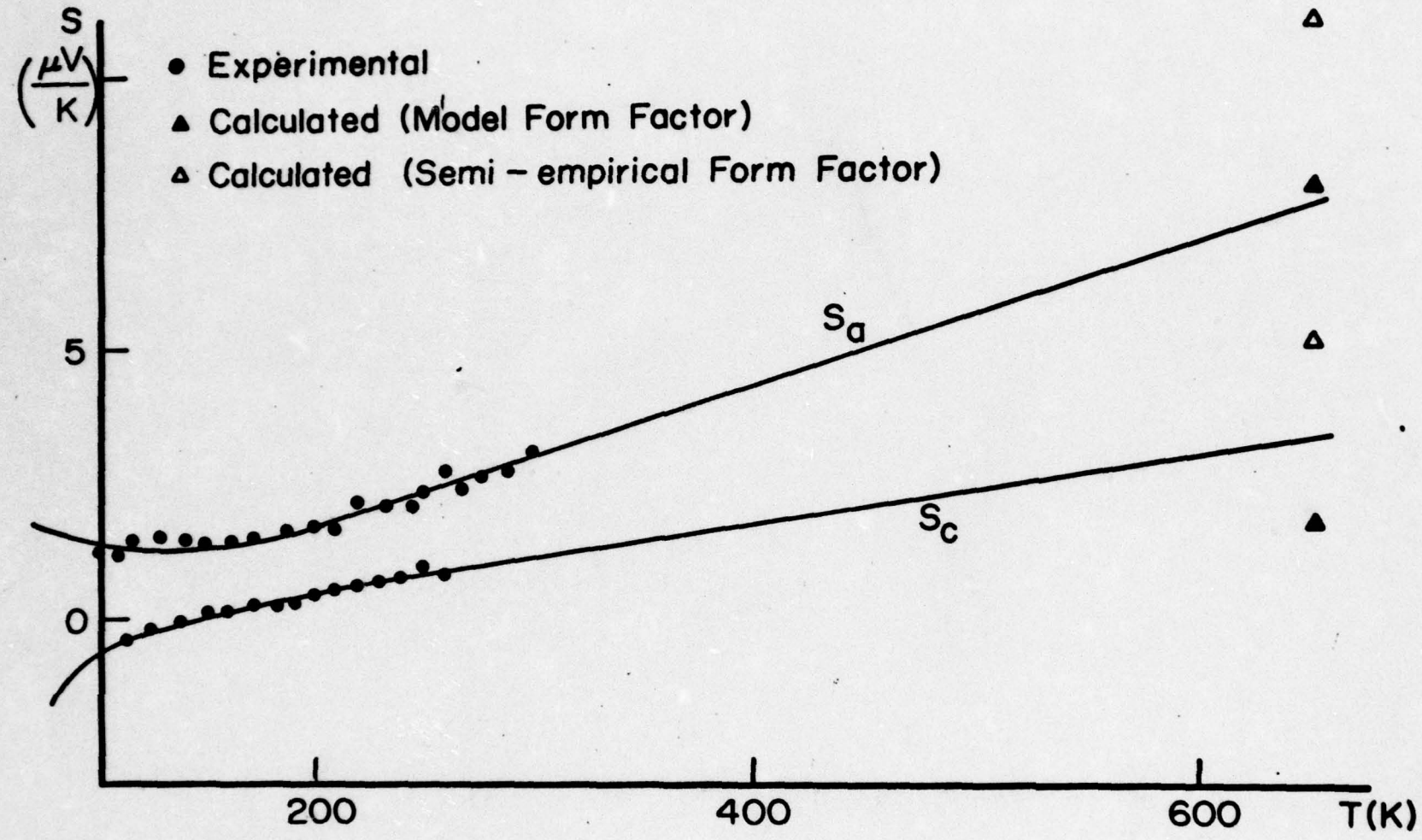

Fig. 4.4: Thermopower vs. Temp.

calculations appear to agree qualitatively with experiment. The contributions of the individual terms s_1 and s_2 will be discussed in the next section.

PART V

DISCUSSION AND CONCLUSIONS

This work has dealt with the calculation of the high temperature transport parameters of single crystal Zn. Zn is a divalent metal, but has small band gaps; consequently, we have employed a 2-OPW NFEM (APPENDIX B). Fermi surface experiments indicate that the third band "butterflies" in Zn are unoccupied. This is consistent with our model (missing area) which predicts that they remain unoccupied, even at high temperature. We have also used a local pseudopotential approximation, which, as discussed in APPENDIX A, is adequate for the calculation of transport properties. Such a model is able to account for the high temperature conductivity of Zn;[22] our calculations have demonstrated its applicability to a variety of other transport phenomena. Cd exhibits similar transport property anisotropy, so that much of the discussion below applies qualitatively to Cd as well.

A. Driving Force for Electromigration

In PART II.A., we have reconsidered band structure effects in electromigration by calculating the driving force on a weak scattering impurity in a drifting gas of Bloch electrons. Our approach differs from previous treatments in that we explicitly include directional effects in conduction electron screening via a self-consistent calculation of the scattered electron wavefunctions. As a result, our formal expression for the driving force, Eq. (2.48), depends explicitly on the dielectric matrix. Although we have introduced $\overleftrightarrow{\epsilon}$ in a formal way, in our numerical computations we have not gone beyond the approximation

of treating $\overleftrightarrow{\epsilon}$ as a scalar. In this limit, our formula reduces to those of Feit and Fiks, except for the restriction they impose by treating the migrating atom as if it were in a plane wave state. In the limit of vanishing lattice potential, Eq. (2.48) agrees with the result of Sorbello.

The agreement between our calculated values and experiment must be considered quite good, even though the predicted anisotropy is somewhat low. There is, unfortunately, a certain amount of arbitrariness in some of the factors which contribute to the computed values of Z^*. First, although we calculate Z_w, in order to compare with experiment we assume that $Z_e = +2$, corresponding to the full electrostatic force being present. Although we feel this is essentially correct, it remains a somewhat controversial question. Second, the values of $\langle \tau_i \rangle$ are taken from an independent solution of the Boltzmann equation. However, since they are approximately consistent with the experimental conductivity, they might alternatively be considered as empirically determined parameters. In fact, closer agreement with the experimental anisotropy would have been obtained if the relaxation times had been fitted to the actual experimental conductivity values. Finally, the calculated values of Z_w are of course dependent on choice of pseudopotential form factor. The use of the model form factor (dotted line in Fig. A.1), for example, yields values roughly 30-40 per cent greater than those shown in Table 2.1.

Despite the qualifications discussed in the previous paragraph, several unambiguous conclusions emerge from the numerical computations. Quite clearly, the anisotropy in effective charge is due primarily to the anisotropy in relaxation times. Unlike the conductivity calculation,

where Fermi surface distortion compensates the anisotropic relaxation times quite closely, only a slight compensation occurs in the electron wind force. We find that $Z_w^a/Z_w^c = 1.35$, compared to $\langle\tau_a\rangle/\langle\tau_c\rangle = 1.65$. This confirms the suggestion of Chan and Huntington[22] based on rough estimates of the wind forces.

Table 2.1 also points out the magnitude of the various band structure effects which we have considered. The effect of the missing Fermi surface area is quite drastic since the wind force formula involves two integrations over the Fermi surface. Another result of Fermi surface distortion is the vanishing normal component of electron velocity (and mean free path) at a zone boundary; this tends to reduce transport perpendicular to the zone boundary. There is also the fact that Bloch waves are not momentum eigenfunctions, so that a given scattering event does not give rise to a well defined momentum transfer. In terms of free electrons, an electron may be simultaneously scattered by the defect and Bragg reflected. We find that this also tends to decrease the effective charge.

We should also comment on the effect of defect structure in the case of vacancy diffusion. Although the full calculations were not repeated for an isolated point defect, some preliminary calculations indicate that the effective charge for the vacancy case is roughly 30 per cent lower than for the interstitial case.

B. Hall Effect

At 650 K, our calculated value for $R_{\parallel}$ is roughly 1.5 times the free electron value for Zn in magnitude, and opposite in sign. This large positive value is due to the regions of negative curvature in the

"monster" section of the Fermi surface, i.e., to the region between horizontal (002) Brillouin zone planes. In our model, this region is strongly distorted by the slanting (101) zone planes. Fig. B.2 indicates the reversal of curvature below the BZ intersections. The free electron-like "lens" (polar caps), on the other hand, has positive curvature and contributes toward a negative Hall constant. Compensation between regions of opposite curvature result in a small, negative value for $R_{\perp}$.

As discussed in PART III, our numerical values depend on the somewhat arbitrary division of the free Fermi surface area into regions (Fig. B.3). Although our choice of boundaries based on the Onsager symmetry requirements seems physically reasonable, it would be more satisfying to have a model without this degree of arbitrariness. The $R_{\perp}$ calculation turned out, in fact, to be quite sensitive to the precise choice of boundaries owing to close cancellation between positive and negative contributions. The $R_{\parallel}$ calculation, however, proved to be nearly independent of this choice. The same conclusion can be drawn concerning the neglect of the $\vec{\nabla}\tau$ term in Eq. (3.18). For $R_{\perp}$, the close cancellation between "curvature" contributions shows that the $\vec{\nabla}\tau$ term is quantitatively important for $R_{\perp}$. On the other hand, our analysis shows that it is negligible for $R_{\parallel}$.

We have explained the temperature dependence of the Hall effect within our model in terms of changing Fermi surface-Brillouin zone wall interactions, as suggested by Stringer, et. al.[87] for Cd. The changing c/a ratio (Table 3.1) shifts the zone planes with respect to the Fermi sphere. For example, γ_{002} decreases with temperature,

increasing the relative size of the free electron-like "lens". The dominant temperature dependence in our model derives from the reduction in band gaps . Quite simply, increasing the temperature reduces Fermi surface distortion through the band gap parameter g, driving the Hall constants in the negative direction. These effects appear adequate to explain the observed temperature dependence (Fig. 3.1), although we cannot rule out completely the effect of temperature dependent anisotropic relaxation times, particularly for $R_\perp$.

C. Thermoelectric Power

Our calculated values of τ_i vs. μ provide a good check on the model and method of computation used in this section. Fig. 4.3 is in qualitative agreement with Fig. C.3 from Ref. 22; the lower average values obtained here being due to the simplified model we used. However, since we are interested primarily in the energy derivatives of the relaxation times, and not on their actual values, this disagreement does not appear serious.

We find $\frac{\partial \langle \tau_i \rangle}{\partial \epsilon}$, and consequently s_{2i}, to be negative, contributing toward a positive thermopower. As in the noble metals, this is due primarily to the fact that the form factor has its first node at a wavenumber less than $2k_F$, so that the scattering cross section (depending on F^2) becomes a minimum at this point and then increases again beyond the node. This results in an increase in back scattering (large values of $|\vec{k}'-\vec{k}|$) probability as energy increases; such processes dominate the resistivity in the high temperature (umklapp) regime. As might be expected, this term proved to be very sensitive to the exact shape of the form factor used.

Our model (Fig. 4.1) obviously provides only a very rough treatment of the effects of Fermi surface distortion, since it includes only the missing area correction. As the Fermi surface expands outward (i.e., ϵ increases) against the slanting Brillouin zone planes, the amount of missing area is increased, and the integrals X_i correspondingly reduced. The missing area is concentrated nearer the basal plane, as reflected in the anisotropy in the parameter s_1 (Table 4.1). An independent calculation of only the s_1 terms, but taking full Fermi surface distortion into account using the 2-OPW model surface of APPENDIX B, yielded $s_{1a} = -5.4$ and $s_{1c} = +.37$. These values are in rough agreement with those in Table 4.1, the differences pointing out the approximate nature of the models and the sensitivity of the calculation. Nevertheless, the s_1 factor does qualitatively account for the experimentally observed anisotropy in S_i. Also, the sums of the s_1 and s_2 factors result in values of S_a and S_c which appear consistent with experimental values at lower temperatures (Fig. 4.4).

PART VI

LITERATURE CITED

1. P. Drude, Ann. Phys., Lpz. 4, 1, 566(1900).
2. H. A. Lorentz, Proc. Acad. Sci. Amst. 7,438, 535, 684(1904).
3. A. Sommerfeld, Z. Phys. 47, 1(1928).
4. J. M. Ziman, Theory of Solids, (Cambridge University Press, 1964), p. 182.
5. N. F. Mott and H. Jones, The Properties of Metals and Alloys, (Clarendon Press, Oxford, 1936), p. 261.
6. J. M. Ziman, Phys. Rev. 121, 1320(1961).
7. J. S. Dugdale and Z. S. Basinski, Phys. Rev. 157, 552(1967).
8. R. D. Barnard, J. E. A. Alderson, T. Farrell, and C. M. Hurd, Phys. Rev. 176, 761(1968).
9. T. Matsuda, J. Phys. Chem. Solids 30, 859(1969).
10. I. Giaever, Ph. D. thesis, Rensselaer Polytechnic Institute, 1964,(unpublished).
11. P. T. Truant and J. P. Carbotte, Solid State Commun. 11, 443(1972).
12. P. L. Taylor, Proc. Roy. Soc. London A275, 209(1963).
13. J. M. Ziman, Electrons and Phonons, (Clarendon Press, Oxford, 1960), p. 275.
14. R. C. Dynes and J. P. Carbotte, Phys. Rev. 175, 913(1968).
15. E. Borchi, S. De Gennaro, and P. I. Taselli, Phys. Status Solidi B 46, 489(1971).
16. P. Pecheur and G. Toussaint, J. Phys. Chem. Solids 33, 2281(1972)
17. J. E. Robinson and J. D. Dow, Phys. Rev. 171, 815(1968).
18. P. J. Price, IBM J. Res. Develop. 1, 239(1957).
19. P. L. Taylor, Proc. Roy. Soc. London A275, 200(1963).
20. C. Herring and F. Vogt, Phys. Rev. 101, 944(1956).

21. W. C. Chan and H. B. Huntington, Phys. Rev. B 12, 5423 (1975).

22. W. C. Chan and H. B. Huntington, Phys. Rev. B 12, 5441(1975).

23. J. C. Phillips and L. Kleinman, Phys. Rev. 116, 287(1959).

24. W. A. Harrison, Pseudopotentials in the Theory of Metals, (W. A. Benjamin, Inc., New York, 1966).

25. B. N. Aleksandrov and I. G. D'Yakov, Zh. Eksp. Teor. Fiz. 43, 852(1962). (Sov. Phys. - JETP 16, 603(1963).)

26. J. E. A. Alderson and C. M. Hurd, Phys. Rev. B 12, 501(1975).

27. V. B. Fiks, Soviet Phys. Solid State 1, 14(1959).

28. H. B. Huntington and A. R. Grone, J. Phys. Chem. Solids 20, 76(1961).

29. C. Bosvieux and J. Friedel, J. Phys. Chem. Solids 23, 123(1962).

30. R. S. Sorbello, J. Phys. Chem. Solids 34, 937(1973).

31. A. K. Das and R. Peierls, J. Phys. C: Solid State Phys. 6, 2811(1973).

32. P. Kumar and R. S. Sorbello, Thin Solid Films 25, 25(1975).

33. W. L. Schaich, preprint.

34. L. J. Sham, preprint.

35. R. Kubo, J. Phys. Soc. (Japan) 12, 570(1957).

36. V. B. Fiks, Soviet Phys. Solid State 6, 1251(1964).

37. V. B. Fiks, in Atomic Transport in Solids and Liquids, ed. A. Lodding and T. Lagerwall, Verlag der Zeitschrift fur Naturforschung, Tubingen (1971), p. 3.

38. H. B. Huntington, W. B. Alexander, M. D. Feit, and J. L. Routbort, in Atomic Transport in Solids and Liquids, p. 91.

39. J. L. Routbort, Phys. Rev. 176, 796(1968).

40. H. Jones and C. Zener, Proc. Roy. Soc. A145, 268(1934).

41. J. M. Ziman, Adv. Phys. 10, 1(1961).

42. G. S. Lane, A. S. Huglin, and J. Stringer, Phys. Rev. 135, 1060(1964).

43. K. Yonemitsu and S. Takahashi, J. Phys. Soc. (Japan) 27, 352(1969).

44. P. H. Cowley and J. Stringer, Phil. Mag. 29, 99(1974).

45. R. S. Allgaier, Phys. Rev. 158, 699(1967).

46. R. S. Allgaier, Phys. Rev. 165, 775(1968).

47. Ref. 5, p. 310.

48. Ref. 13, p. 409.

49. J. M. Ziman, Proc. Roy. Soc. A252, 636(1959).

50. J. E. Robinson, Phys. Rev. 161, 533(1967).

51. J. Yamashita and S. Asano, Prog. Theor. Phys. 50, 1110(1973).

52. O. Dreirach, J. Phys. F 3, 577(1973).

53. J. E. Black, Phys. Status Solidi B 66, K83(1974).

54. O. K. Kuvandik, A. V. Cheremus, and R. P. Vasileva, Phys. Met. R. 34, 186(1972).

55. V. A. Rowe and P. A. Schroeder, J. Phys. Chem. Solids 31, 1(1970).

56. C. M. Hurd, Adv. Phys. 23, 315(1974).

57. R. W. Stark and L. M. Falicov, Phys. Rev. Letters 19, 795(1967).

58. H. Ehrenreich and M. H. Cohen, Phys. Rev. 115, 786(1959).

59. D. S. Falk, Phys. Rev. 118, 105(1960).

60. H. B. Huntington, Trans. AIME 248, 2571(1969).

61. P. C. Mangelsdorf, J. Chem. Physics 33, 1151(1960).

62. R. Landauer and J. W. F. Woo, Phys. Rev. B 10, 1266(1974).

63. R. Landauer, J. Phys. C 8, 761(1975).

64. R. Landauer, IBM J. Res. Develop. 1,223(1957).

65. R. Landauer and J. W. F. Woo, Phys. Rev. B 5, 1189(1972).

66. R. S. Sorbello, Comments Sol. State Phys. 6, 117(1975).

67. M. J. Bibby and R. Youdelis, Canad. J. Phys. 44, 2363(1966).

68. L. Turban, P. Nozieres, and M. Gerl, preprint.

69. A. Messiah, Quantum Mechanics, (John Wiley and Sons, New York, 1958), p. 786.

70. E. Merzbacher, Quantum Mechanics, (John Wiley and Sons, New York, 1970), p. 498.

71. J. C. Stoddart, N. H. March and M. J. Stott, Phys. Rev. 186, 683(1969).

72. L. J. Sham and J. M. Ziman, Solid State Physics 15, (Academic Press Inc., London, 1963), p. 270.

73. Ref. 24, p. 46.

74. R. S. Sorbello, Ph. D. thesis, Stanford University, 1970, (unpublished).

75. See for example, S. Adler, Phys. Rev. 126, 413(1962) and N. Wiser, Phys. Rev. 128, 2093(1962).

76. S. K. Sinha, CRC Critical Reviews in Solid State Physics 3, 273(1972).

77. S. R. de Groot, Thermodynamics of Irreversible Processes, (North Holland Publishing Co., Amsterdam, 1951), p.50.

78. M. M. Noskov, Zn. Eksperim. i Teor. Fiz. 8, 717(1938).

79. J. K. Logan and J. A. Marcus, Phys. Rev. 88, 1234(1952).

80. H. M. Gilder and G. N. Wallmark, Phys. Rev. 182, 771(1969).

81. W. C. Chan, Ph. D. thesis, Rensselaer Polytechnic Institute, 1974, (unpublished).

82. F. J. Blatt, Physics of Electronic Conduction in Solids, (McGraw-Hill, New York, 1968), p. 148.

83. Numerical values provided by P. Pecheur, private communication.

84. A. J. Greenfield and N. Wiser, J. Phys. F 5, 1289(1975).

85. E. F. Skelton and J. L. Katz, Phys. Rev. 171, 801(1968).

86. L. E. Enderby, Proc. Roy. Soc. 81, 772(1963).

87. J. Stringer, I. Hill, and A. Huglin, Phil. Mag. 1, 53(1970).

APPENDIX A

DISCUSSION OF FORM FACTOR

The pseudopotential method in the theory of simple metals is discussed in detail by Harrison.[24] His formulation is based on the Orthogonalized Plane Wave (OPW) method in which the basis functions for expansion are plane waves whose projections onto the core states have been eliminated to insure orthogonality between core and conduction states. Lumping the core projection operators into the potential provides a repulsive term, cancelling part of the coulomb attraction term. The resulting pseudopotential is weak (allowing the use of first order perturbation theory) though non-local; i.e., its matrix elements between states $\vec{k}$ and $\vec{k}'$ in general depend on $\vec{k}$ and $\vec{k}'$, and not just on $q = |\vec{k} - \vec{k}'|$. In the calculation of transport properties, however, we are interested only in scattering on a constant energy shell, and the error introduced by treating the effective potential as local is small.

The solid line in Fig. A.1 shows the form factor for Zn[83] calculated by a semi-empirical method. The scheme involves interpolation between points determined by Stark and Falicov[57] from their analysis of low temperature Fermi surface measurements, i.e., de Haas-van Alphen effect data. Calculation of the core repulsion contribution to the pseudopotential is also described in Ref. 57. A recent form factor calculation by Greenfield and Wiser[84] agrees quite well with the values which we used. In numerical computation, we used the analytic expression

$$F(q) = A \frac{\sin(Bq/k_F)}{(q/k_F)} + C \sin^2(Dq/k_F) \quad , \qquad (A.1)$$

with A = -2.49 rydbergs, B = 1.85, C = .046 rydbergs, and D = 2.03. The analytic form fit the semi-empirical values to within about .01 rydbergs. Also shown in Fig. A.1 is the model form factor used by Chan and Huntington[22] in the calculations described in APPENDIX C. This is given by the functional form

$$F(q) = F_0(1 - q^2/2.9\, k_F^2) \quad , \tag{A.2}$$

with F_0 = -.34 rydbergs.

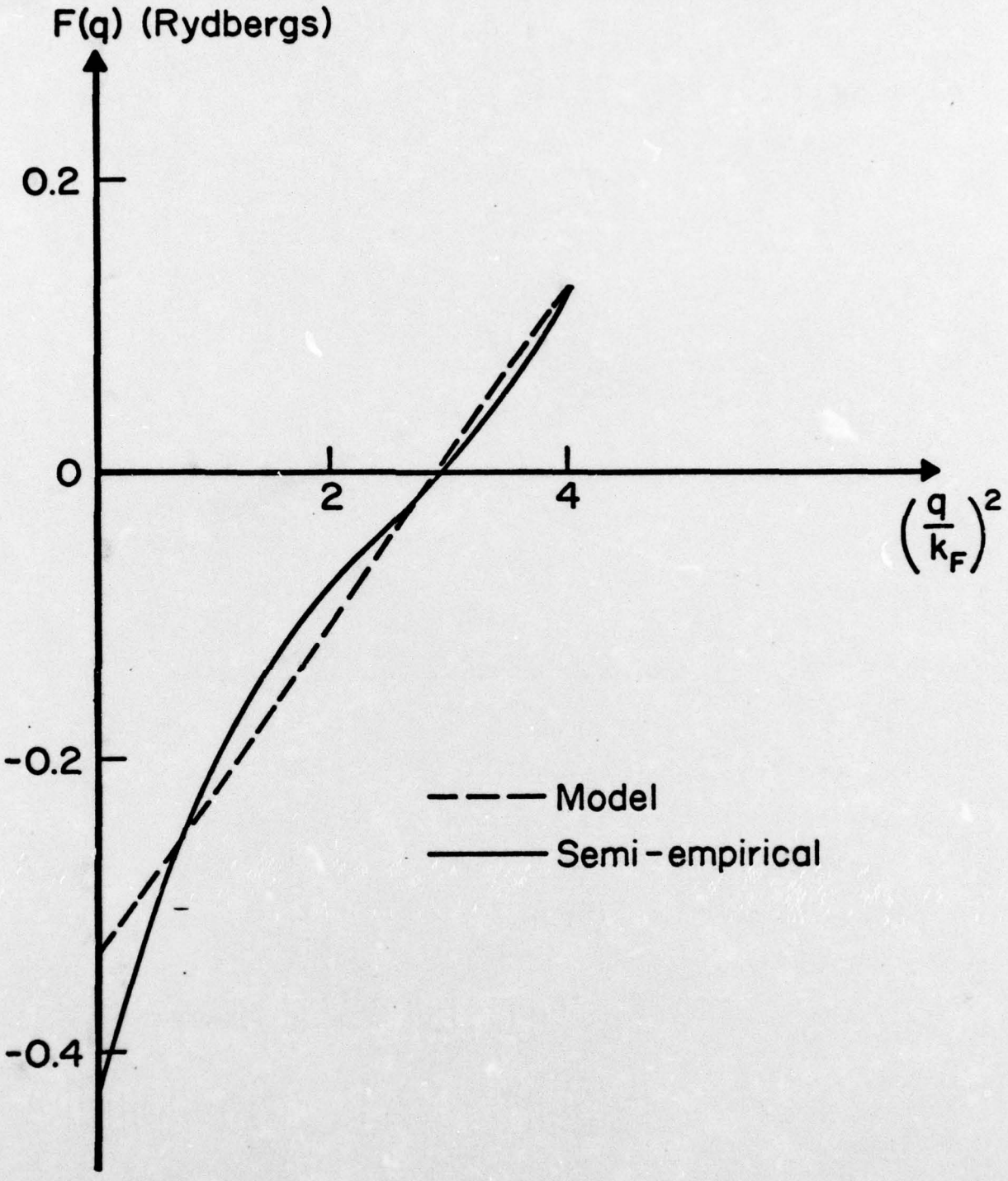

Fig. A.1: Form Factors for Zn

APPENDIX B
FERMI SURFACE MODEL

The Fermi surface of Zn is distorted by three sets of Brillouin zone planes whose RLV's are the vectors $\vec{Q}_1$, $\vec{Q}_2$ and $\vec{Q}_3$ of Eqs. (4.17). (We switch to the notation $\vec{K}_i$, reserving $\vec{Q}$ for electron phonon umklapp.) The amount of distortion caused by each plane is determined by the coupling strength parameter, $g = k_F |F(K)| / \epsilon_F K$ (see Eq.(B.1)). The relevant g values for Zn at 650 K are given below.

	$\lvert\vec{K}\rvert (k_F)$	g
$\vec{K}_1$	1.596	.023
$\vec{K}_2$	1.740	.001
$\vec{K}_3$	1.914	.047

Table B.1 : Coupling Strength Parameters

The tabulated values include a correction for the Debye-Waller factor,[85] which effectively reduces the band gaps with temperature. The table reveals two important points. First, the wavenumbers of the Brillouin zone planes that intersect the Fermi sphere fall in the region where the form factor (Fig. A.1) is relatively small; i.e., the region where cancellation between Coulomb attraction and core repulsion terms in the pseudopotential is close. This results in small band gaps and a NFE band structure. Second, the K_2 RLV falls very near the zero of F(q). We will therefore ignore the distortion caused by this set of planes, which results in considerable simplification.

Fig. B.1(a) shows the Jones (or second Brillouin) zone for Zn, and Fig. B.1(b) depicts the intersections of the Fermi sphere with

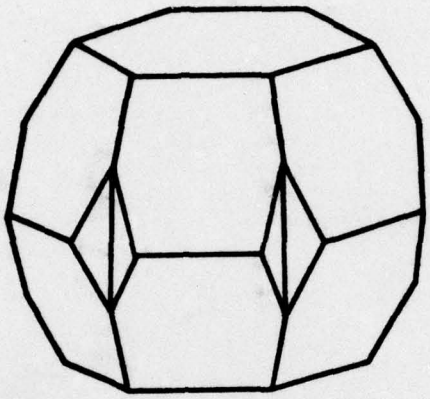

(a) Jones Zone

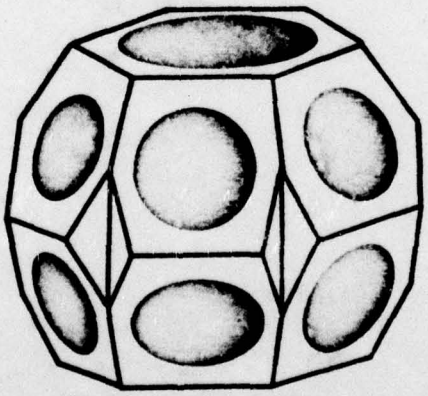

(b) Fermi Sphere Intersections

Fig. B.1: Intersection of Fermi Sphere With Jones Zone

the planes determined by the sets of vectors $\vec{K}_1$ and $\vec{K}_3$. We treat the effects of distortion of one pair of planes at a time, as illustrated in Fig. B.2. In this 2-OPW model, the equation

$$\frac{\epsilon}{\epsilon_F} = \left(\frac{k}{k_F}\right)^2 + 2\gamma\left\{(\gamma-\mu) \pm \left[(\gamma-\mu)^2 + g^2\right]^{\frac{1}{2}}\right\} \qquad \text{(B.1)}$$

gives the electron energy near the Kth zone. The plus sign in Eq. B.1 goes with $\mu > \gamma$. Differentiation gives the electron velocity near the Kth zone:

$$v_{\parallel} = \frac{\hbar k_F}{m}\left\{\mu - \gamma\left[1 - \frac{|\gamma-\mu|}{\sqrt{(\gamma-\mu)^2 + g^2}}\right]\right\} \qquad \text{(B.2)}$$

$$\equiv \frac{\hbar k_F}{m}\left[\mu - 2\gamma\beta^2(\mu)\right]$$

$$\simeq \frac{\hbar k_F}{m}\mu\left[1 - 2\beta^2(\mu)\right] = \frac{\hbar k_F}{m}\frac{\mu|\gamma-\mu|}{\sqrt{(\gamma-\mu)^2 + g^2}}, \qquad \text{(B.3)}$$

$$v_{\perp} = \frac{\hbar k_F \rho}{m} . \qquad \text{(B.4)}$$

Eq. (B.1) also reveals that for the slanting, or K_3 RLV's, the values of γ and g are such that the region corresponding to $\mu > \gamma$ is not occupied. This results in a considerable amount of missing free area from the Fermi surface, as illustrated by the shaded areas in Fig. B.3. Fig. B.3 also illustrates the division of the surface into regions in which the effect of a single pair of planes is considered. In the computations, each of the regions bounded by dotted lines was approximated by a region of equal area, but cylindrically symmetric about the appropriate RLV.

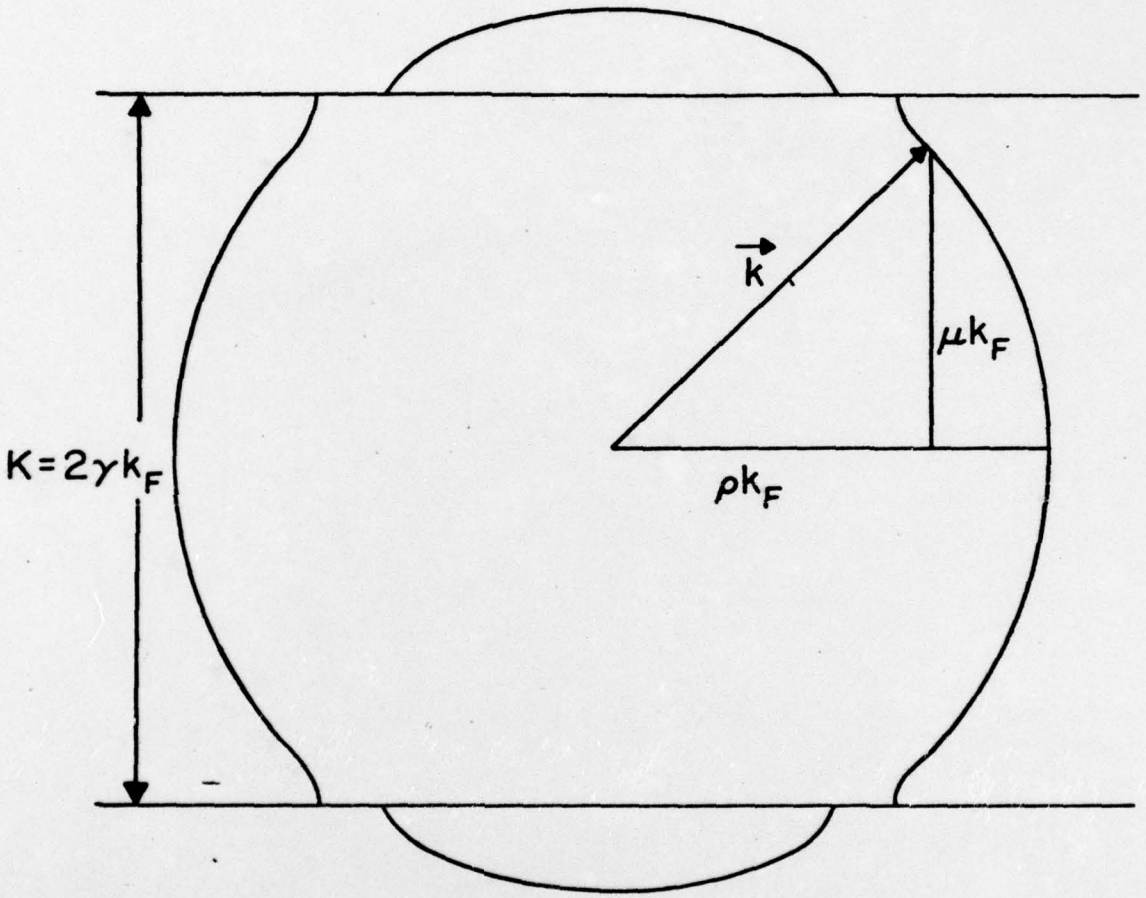

Fig. B.2: Distortion of Fermi Sphere by a Single Pair of Brillouin Zone Planes

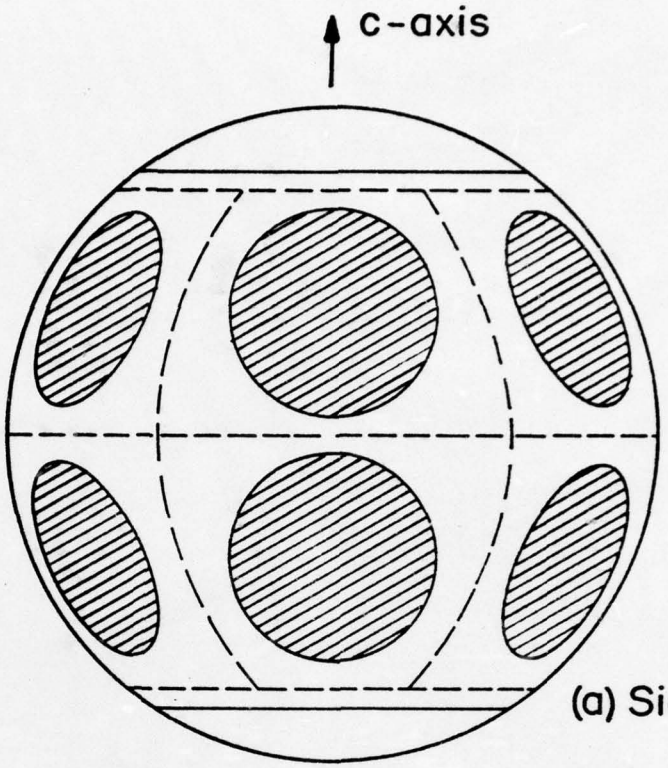

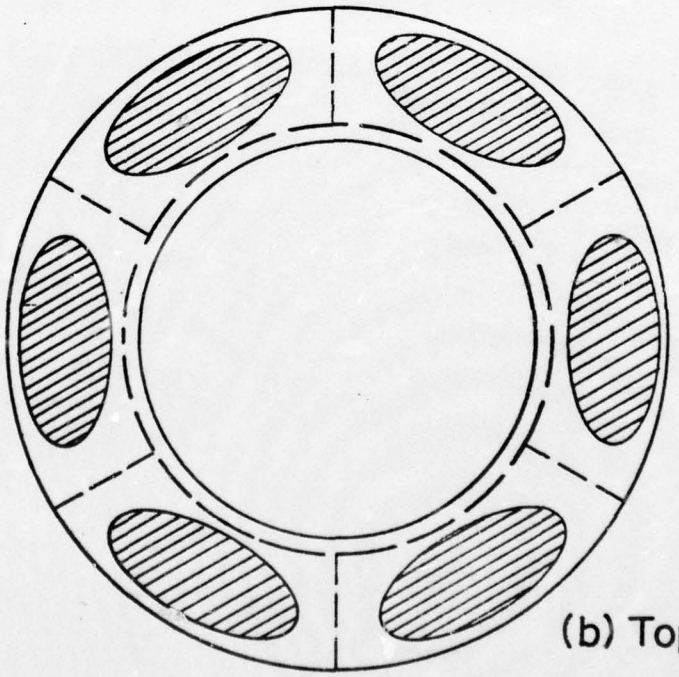

Fig. B.3: Division of Fermi Surface Into Regions

APPENDIX C

SOLUTION OF THE BOLTZMANN EQUATION

We present here a summary of the Chan and Huntington[22] solution of the Boltzmann equation (Eq. (4.3)) for the vector mean free path $\vec{\lambda}$. Briefly, they write each component of $\vec{\lambda}$ in the form $\lambda_i = \tau_i v_i$, and then develop an iterative scheme for the relaxation time τ_i. The transition probability $W(\vec{k},\vec{k}')$ is dominated by the electron-phonon interaction in the high temperature regime. Experimental phonon dispersion curves are shown in Fig. C.1. These are used to derive an approximate set of dispersion curves, each applicable to umklapp processes involving a particular RLV. (Normal processes are handled similarly.) These fitted dispersion curves are shown in Fig. C.2.

Results for $\langle\tau_c\rangle$ and $\langle\tau_a\rangle$ (corresponding to the $\vec{E}$ field being applied parallel and perpendicular to the c-axis, respectively) are shown in Fig. C.3. The phonon dispersion curves show that acoustic velocities are lower for modes polarized perpendicular to the basal plane. As a result, the electron scattering is greater for the umklapp processes parallel to the c-axis, and the relaxation time is thus shorter for conduction in the c direction. However, distortion of the Fermi sphere and the resulting missing area discussed in APPENDIX B has a greater effect on conduction in the a direction. The Fermi surface distortion compensates quite closely the elastic anisotropy, giving a nearly isotropic conductivity in good agreement with experiment.

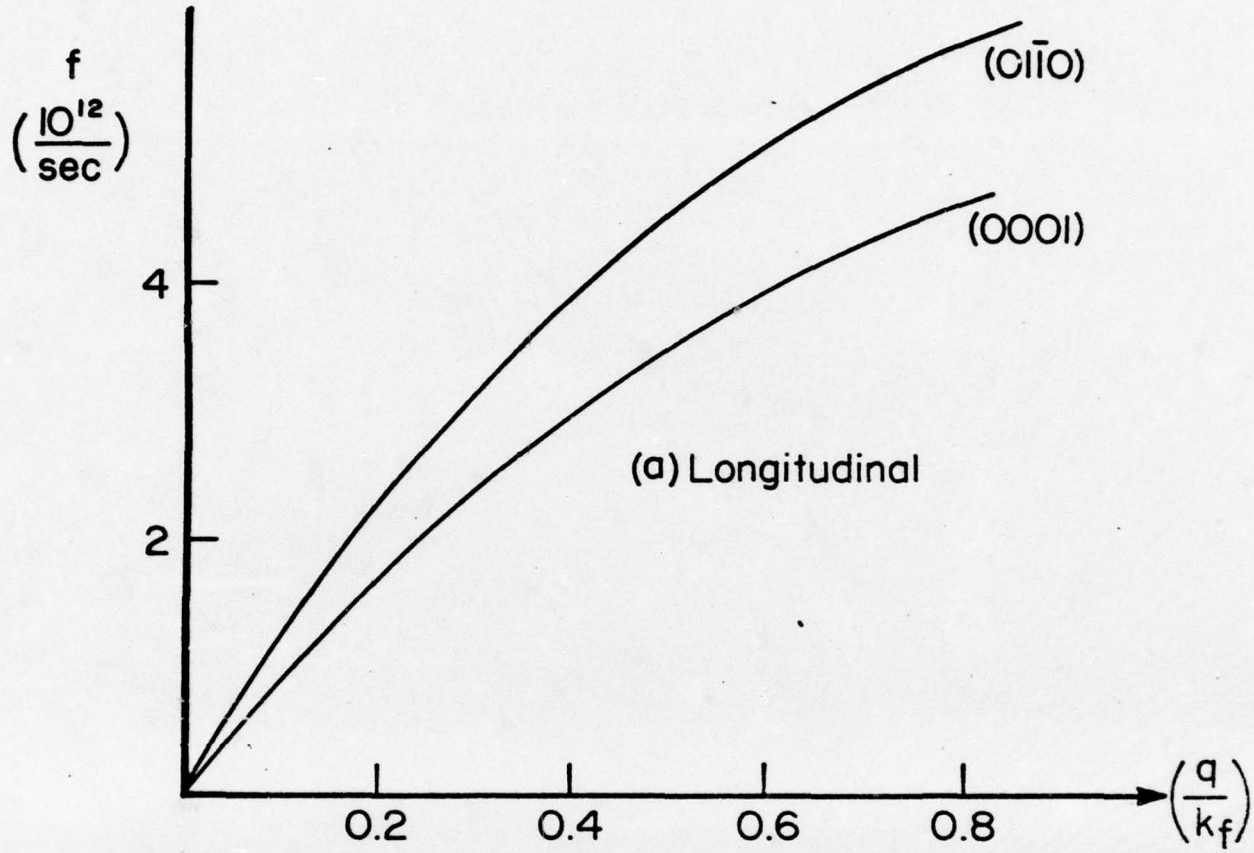

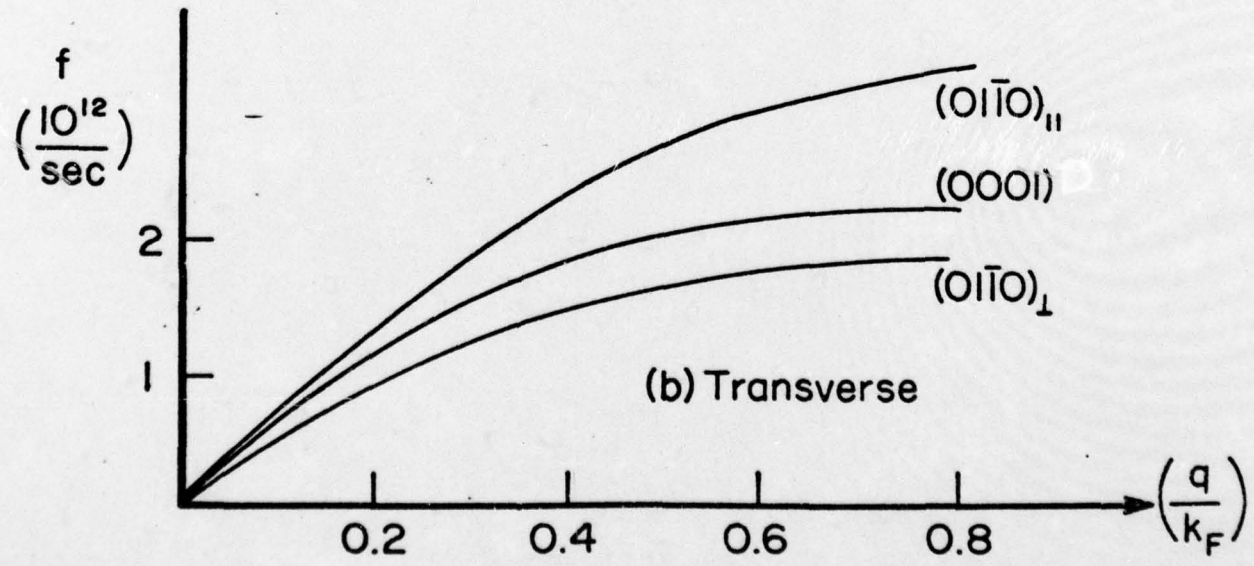

Fig. C.1: Experimental Phonon Dispersion Curves

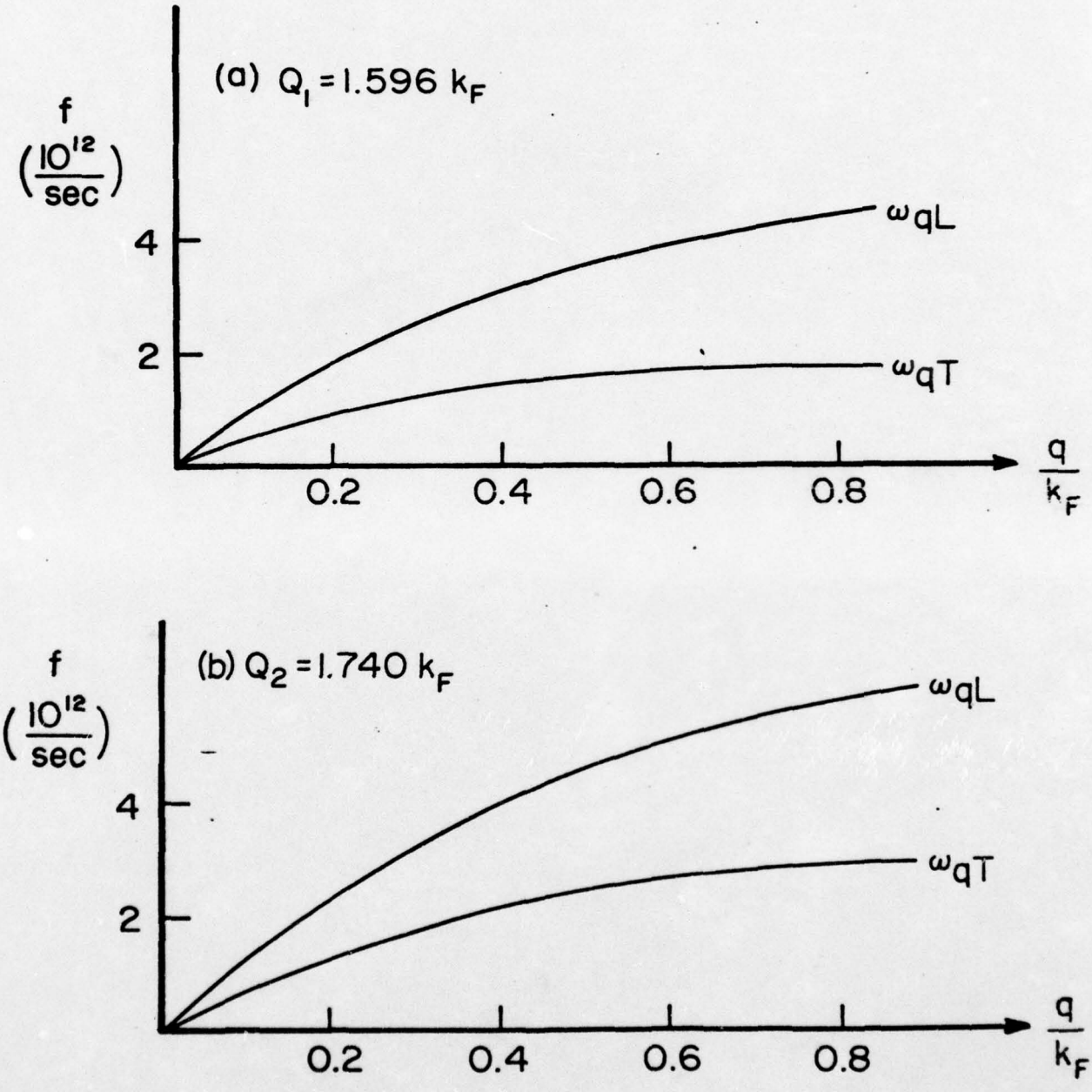

Fig. C.2: Phonon Dispersion Curves (Analytic Fits)

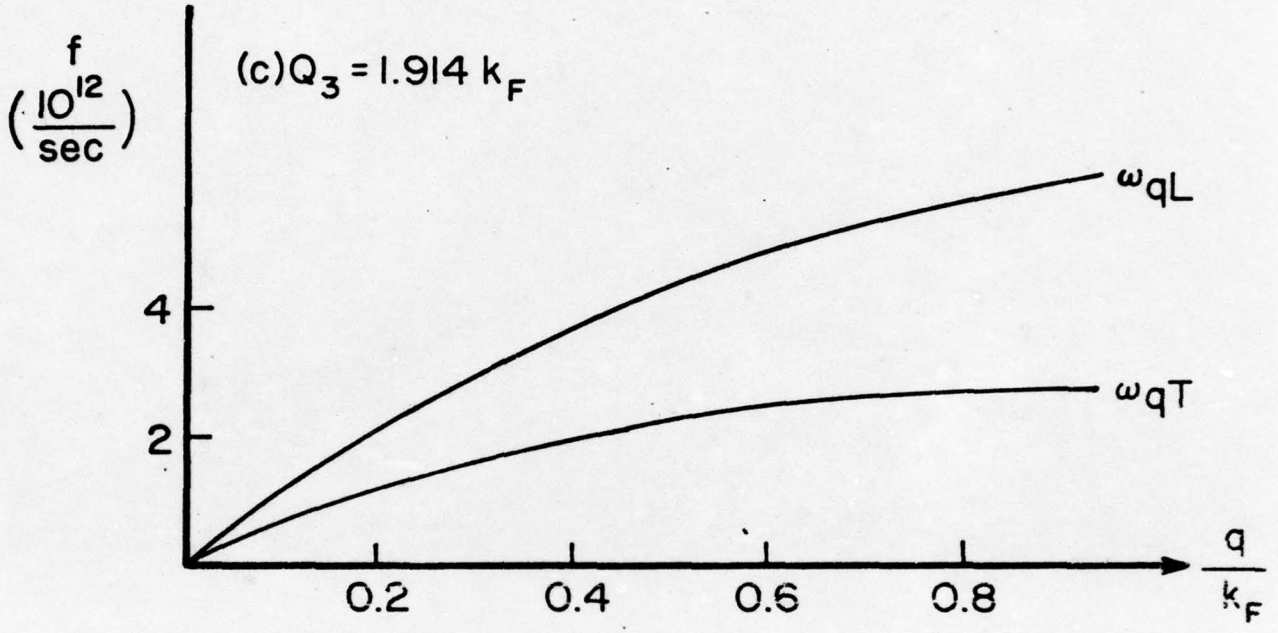

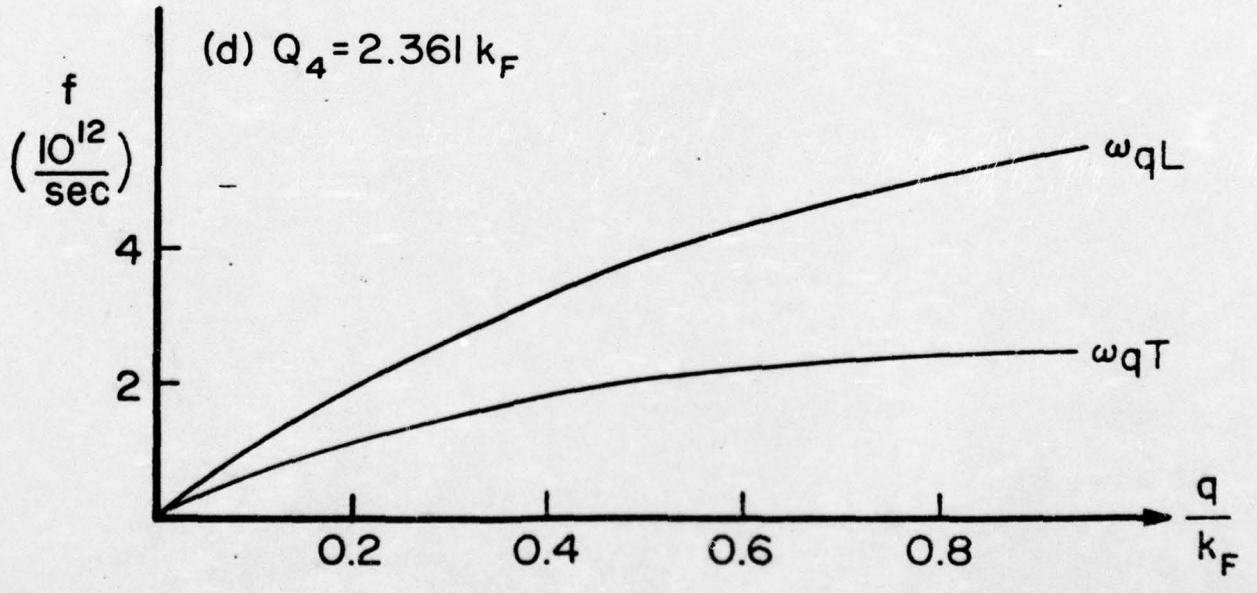

Fig. C.2: (continued)

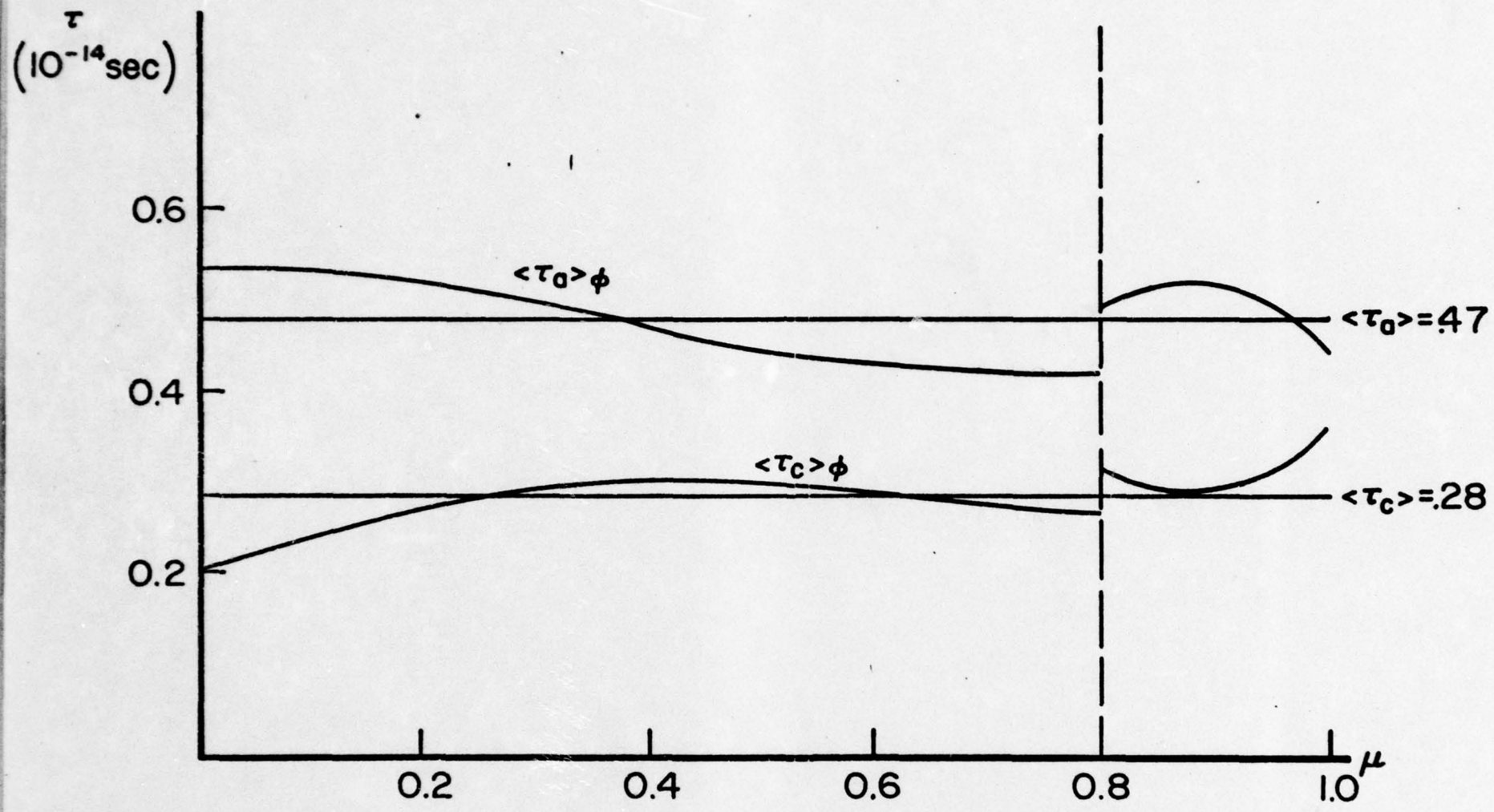

Fig. C.3: $\langle \tau_i \rangle$ vs. μ (Calculated in Ref. 22)